# UPPER MANTLE SHEAR VELOCITY STRUCTURE OF EAST AFRICA, THE ARABIAN SHIELD, AND THE EASTERN MEDITERRANEAN

by

Mary K. DuPass

---

A Thesis Submitted to the Faculty of the

DEPARTMENT OF GEOSCIENCES

In Partial Fulfillment of the Requirements
For the Degree of

MASTER OF SCIENCE

In the Graduate College

THE UNIVERSITY OF ARIZONA

1 9 8 9

## STATEMENT BY AUTHOR

This thesis has been submitted in partial fulfillment of requirements for an advanced degree at The University of Arizona and is deposited in the University Library to be made available to borrowers under rules of the library.

Brief quotations from this thesis are allowable without special permission, provided that accurate acknowledgment of source is make. Requests for permission for extended quotation from or reproduction of this manuscript in whole or in part may be granted by the head of the major department or the Dean of the Graduate College when in his or her judgment the proposed use of the material is in the interests of scholarship. In all other instances, however, permission must be obtained from the author.

SIGNED Mary K DuPass

## APPROVAL BY THESIS DIRECTOR

This thesis has been approved on the date shown below:

Terry C. Wallace

Terry C. Wallace
Associate Professor of Geosciences

3-8-89
Date

# ACKNOWLEDGMENTS

Several people within the Geosciences Department have helped make my time at the University of Arizona be both an educational and an enjoyable experience. I would particularly like to thank Terry Wallace for his guidance and encouragement throughout the completion of this program and Clem Chase and Randy Richardson for their reviews of my work and their many helpful suggestions. I am also grateful to Bill Holt, Liz Greene, and Charles Williams for making all of those long hours in the computer room seem not quite so long. In addition, I would like to thank Norm Meader for his expert help in setting up the final version of this thesis. Finally, a special thanks goes to Vince Realmuto for his continued support throughout the research and writing of this thesis.

Funding for this project was provided by the Amoco Foundation.

TABLE OF CONTENTS

LIST OF ILLUSTRATIONS

LIST OF ILLUSTRATIONS--Continued

## LIST OF TABLES

## ABSTRACT

Forward modeling of SH-polarized, long-period bodywaves (S and SS) constrains the lateral heterogeneity of the upper mantle seismic velocity structure beneath east Africa, the Arabian shield, and the eastern Mediterranean. The transition from the tectonically active East African Rift Zone to the surrounding continental craton is well resolved. The data set includes 14 earthquakes, 22 raypaths, and 9 WWSSN seismic stations. The traveltime anomalies studied for the different tectonic regimes indicate a direct relation between upper mantle velocities and thermotectonic history and are consistent with velocity models which merge by about 400 km depth. More specifically, shear velocities beneath the African shield are approximately 14.25% higher at 125 km depth, 6.75% higher at 200 km depth, and only 3.5% higher at 300 km depth compared with velocities beneath the most active segments of the rift zone (Kenya and Ethiopia). Seismic velocities beneath the eastern Mediterranean and the Arabian shield are intermediate between these two extremes.

# CHAPTER 1

# INTRODUCTION

Lateral heterogeneity of the upper mantle seismic velocity structure is a well-established global phenomenon. Less certain, however, are the scale of this heterogeneity and the relation between upper mantle velocities and surface tectonic features. Numerous studies have been conducted to examine upper mantle seismic velocities. While most of these studies support the concept of lateral heterogeneity, interpretations of the heterogeneity vary significantly. For example, several surface wave and body wave studies have indicated relatively slow velocities beneath both young oceanic and tectonically active regions, as compared with stable continental cratons (e.g., Toksöz and Anderson, 1966; Woodhouse and Dziewonski, 1984; Grand, 1986; Lerner-Lam and Jordan, 1987). The depth extent of this lateral heterogeneity, however, has been placed anywhere between 200 km and 400 km and in some cases even deeper. While an increased understanding of upper mantle structure is important for the science of seismology, other disciplines of geoscience are affected as well. For instance, the upper mantle velocity structure must be considered when modeling convective systems, chemical evolution of the mantle, or plate dynamics.

Recently, using forward modeling of SH-polarized, long-period S and SS phases and a tomographic inversion technique, Grand (1986) examined the upper mantle shear velocity structure beneath the North American plate. Concentrating on tectonically active western North America, the stable Canadian shield, and the northwest Atlantic, he was able to establish a consistent relation between upper mantle velocities and tectonic history. In particular, he found that the longer the time interval since the last tectonic activity the higher the velocities within the upper 400 km and the thicker the high velocity lid structure within the uppermost mantle. Velocity profile SNA, which has been used to model the velocity structure beneath the Canadian shield (Grand, 1986), includes a lid structure extending to about 155 km depth with a maximum shear velocity of 4.80 km/sec. In addition to the Canadian shield, velocity structure SNA has also been used for the tectonically stable Russian platform and Baltic shield (Rial et al., 1984).

The goal of this study has been to examine the upper mantle shear velocity structure beneath east Africa, the Arabian peninsula, and the eastern Mediterranean. Particular emphasis has been placed on the transition from the tectonically active East African Rift Zone to the surrounding stable craton. Upper mantle shear velocity profiles have been constructed to constrain the scale of lateral heterogeneity. Variations in velocity structure necessary to fit the waveform data show significant trends which can be interpreted as functions of distance to the rift zone. This has involved the forward modeling of long-period S and SS waveforms as recorded at WWSSN (Worldwide Standard Seismic Network) stations within Africa and the Arabian peninsula. The synthetic seismograms were generated using a WKBJ modeling technique which allows for lateral variations in the velocity structure.

Good azimuthal coverage is obtained from the 22 raypaths selected for this study. Most raypaths parallel or cross at least one other raypath, used within the study, providing an additional constraint in the modeling process. In forward modeling, an initial velocity structure is tested by comparing the synthetic waveform with the observed seismic data. The model is adjusted until discrepancies between the observed and synthetic seismograms are minimized, such that the best waveform fit is achieved within the traveltime constraints. The results of this process have been used to construct regional models of both upper mantle velocity distributions and lithospheric thickness for the region of study.

# CHAPTER 2

## REGIONAL TECTONIC SETTING

This chapter briefly discusses the tectonic setting of the African plate and the surrounding region. Information provided here is essential in determining whether a valid correlation exists between thermotectonic history and upper mantle velocities.

The African plate (Figure 1) is bounded on three sides by oceanic ridge systems: the Mid-Atlantic Ocean Ridge to the west, the Southwest Indian Ocean Ridge to the south, and the Indian Ocean Ridge to the east (an alternate view maintains that the East African Rift system is a divergent plate boundary separating the African plate, to the west, from the Somalian plate, to the east). To the northeast, the African plate is bounded by the Red Sea and the Gulf of Aden. A convergent plate boundary separates east Africa and Arabia from the Eurasian plate.

The East African Rift Zone (Figure 2), the world's largest active continental rift system, is one of three rift arms which began development during the breakup of the Afro-Arabian plate. The other two rift arms, the Red Sea and the Gulf of Aden, are floored in part or entirely by oceanic material (Gass, 1970). Rifting within east Africa was initiated at the Afar triple junction, approximately 25 to 40 m.y. ago (see Burke, 1978; Girdler, 1978, 1983), and has since propagated southward at an estimated rate of 2.5 cm/yr (Oxburgh and Turcotte, 1974). The rift follows an approximate north-south trend, splitting into western and eastern arms just north of the equator and reconnecting at about 8 degrees south latitude. The rift activity continues to approximately 20 degrees south latitude.

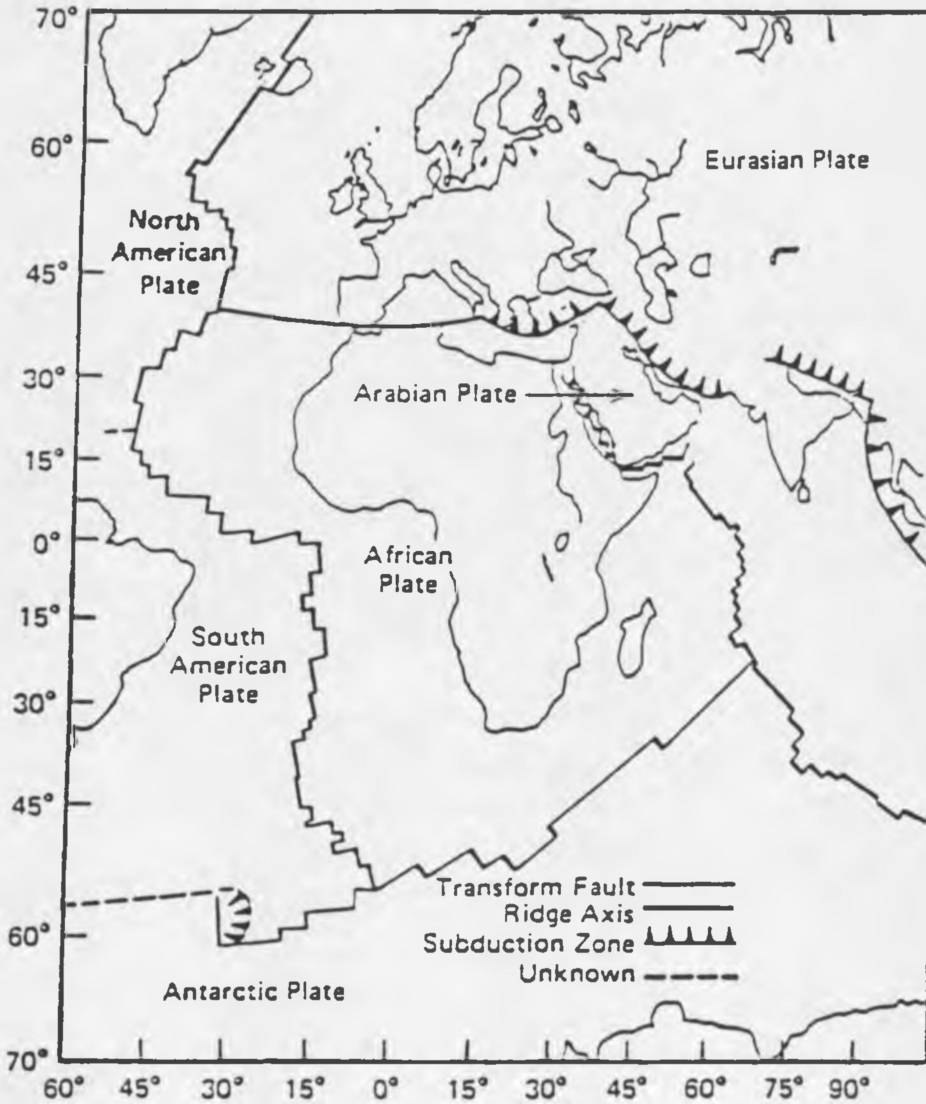


Figure 1. Distribution of plate boundaries surrounding the African continent (after Turcotte and Schubert, 1982).


Figure 2. The East African Rift Zone, the Red Sea, and the Gulf of Aden (after Girdler, 1978).

The East African Rift is characterized by abundant Cenozoic volcanism, doming, and extensional faulting and is the site of a large regional negative Bouguer gravity anomaly, which extends approximately 5000 km in length and 1000 km in width (Girdler, 1978). This negative anomaly, ranging from approximately -50 to -240 mgals (Girdler, 1975), has been attributed to the replacement of lower lithospheric material by slightly less dense, hotter asthenosphere. In Ethiopia and Kenya, a narrow positive anomaly, with an amplitude of 30 to 60 mgals (Girdler, 1978), is superimposed over the rift axes, indicating basaltic intrusions along the rift floors (Logatchev et al., 1983). This and other data indicate that lithospheric thinning (beneath eastern Africa) increases towards the northeast, with the most intense rift activity having occurred along the Kenyan and Ethiopian rift segments. In contrast to this tectonically active province, northwest Africa and south Africa are considered to be relatively stable craton. Burdick et al. (1983) and Grand et al. (1985) have both determined the upper mantle velocity structure beneath the West African craton to be very similar to that beneath the stable Canadian shield. In addition, Chapman and Pollack (1974) have determined lower than average heat flow for this region. They report heat flow measurements of $18 \pm 2$ mW/m$^2$ and $22 \pm 2$ mW/m$^2$ for western Niger. These values are considerably lower than the worldwide shield average of 40 mW/m$^2$. Although much less is known of the Southern African craton, it too is considered to be relatively stable. Chapman and Pollack (1974) report an average heat flow value of 49 mW/m$^2$.

# CHAPTER 3

## FORWARD MODELING TECHNIQUE

Forward modeling of SH-polarized, long-period S and SS waveforms is used in this study of upper mantle velocity structure. The use of SH motion eliminates the complications associated with P-SV coupling while the use of long-period data (as opposed to short-period data) is preferred due to the simplicity of the waveform.

The ability to calculate synthetic seismograms has resulted in an increased understanding of seismic waveforms and has therefore provided greater insight into the finer details of the Earth's internal structure. A synthetic seismogram is created by convolving a series of linear operators which represent the factors affecting the seismogram. In this study, four linear operators have been used. These represent the seismic instrument, attenuation, the seismic source, and wave propagation through the mantle.

The instrument response is well known due to the exclusive use of WWSSN seismic stations. The attenuation operator (a function of $t^*$) can be written as T/Q, the ratio of the average traveltime T to the average quality factor Q. Q is a function of depth and is believed to have its lowest values within the upper few hundred kilometers of the mantle. SS phases, which spend a larger proportion of their traveltime within the uppermost mantle (as compared to S phases), should therefore exhibit a greater amount of attenuation than the associated S waves. The effect of attenuation is generally to smooth the pulse; relative traveltimes should not be significantly altered. The effect of $t^*$, in this study, has been determined by computing several synthetic seismograms with various values of $t^*$. The best average fit to the data occurs when using a $t^*$ value of 4.0 seconds for S waves and a $t^*$ value of 8.0 seconds for SS waves.

The seismic source operator is dependent upon the focal mechanism of the earthquake and is modeled by convolving the effects of the free surface (S-sS interaction) with the source time function. All earthquakes used in this study are moderate-size earthquakes ($m_b$ = 5.3-6.1). A trapezoidal time function which includes rise and fall times of 2.0 seconds each and a rupture time of 3.0 seconds provides the best fit to the average data.

The three linear operators discussed above (instrument response, attenuation, and seismic source) are considered known factors in the forward modeling problem. Therefore, in the calculation of synthetic seismograms, only the upper mantle response requires investigation. The effects of the upper mantle wave propagation, contained within Green's functions, can be approximated by several different methods. Two of the more common methods, generalized ray theory and WKBJ (Wentzel, Kramers, Brillouin, and Jeffreys), are discussed below. A WKBJ approximation is used in this study.

Computing the upper mantle response with the generalized ray theory involves an approximation of the Earth's velocity structure by a series of plane homogeneous layers. The synthetic waveform is then constructed by summing the responses of a finite number of generalized rays which interact with the velocity structure. Of great concern is the minimum set of generalized rays which will provide an accurate approximation of the seismic data. In most cases, the primary ray approximation is sufficient (Burdick and Orcutt, 1979). Even so, the immense amount of computation time involved often renders this method too costly and too impractical for anything but the final stages of modeling.

A significant reduction in computation time results when a WKBJ technique is used to model the effects of upper mantle wave propagation. This method, which essentially utilizes geometric ray theory, assumes a laterally heterogeneous earth structure and offers one of the simplest approximations to the seismic waveform by considering the interaction of only four phases: S, sS, SS, and sSS. Numerical computations involved in the WKBJ technique are discussed by Aki and Richards (1980) and Given (1984).

The WKBJ approximation is most accurate when used for velocity structures with smooth gradients. The approximation breaks down for rays which turn near discontinuities or near very high velocity gradients. All velocity models in this study include a 4.5% increase in velocity at about 405 km depth and an increase of 7.5% at about 659 km depth, both over a 2 km range. Neither velocity increase appears sufficiently steep to significantly alter the modeling results. This becomes particularly evident when reviewing Grand's (1986) comparison of synthetic seismograms which were calculated using both generalized ray theory and WKBJ. Synthetic seismograms were calculated for velocity profiles SNA (stable North America) and TNA (tectonic North America), both of which include the same velocity increases (at 405 km and 659 km depth) described above. In general, the correlation between the two methods is relatively good. Because the WKBJ method does not model the tunneling of energy through the lid nor does it model the amplitude decay off triplication cusps (see Grand, 1986), some differences in response are noted. These discrepancies are more apparent for seismograms constructed with the tectonically stable velocity model, SNA, due to the well-developed high velocity lid structure. Overall, however, the comparison of synthetic waveforms suggests that the WKBJ method provides a sufficiently close approximation to the seismic data for the purposes of this study.

# CHAPTER 4

## DATA

Locations of the 14 earthquakes and 22 raypaths providing constraints on the upper mantle shear velocity structure beneath east Africa, the Arabian peninsula, and the eastern Mediterranean, are shown in Figure 3. The objective was to select a series of raypaths which provide good azimuthal coverage of the region. Most raypaths are paralleled or crossed by at least one other raypath within the study, providing an additional constraint in the modeling process. Earthquake sources are located in Greece, Albania, Turkey, and Iran, and along the Southwest Indian Ocean Ridge. The 14 seismic events are listed in Table 1.

One of the primary goals of this study has been to determine if waveform and traveltime differences, associated with lateral tectonic heterogeneity, can be mapped into velocity structure above 400 km depth. Therefore, all oceanic and continental velocity profiles used here are constructed to be consistent with the assumptions that: 1) variations in seismic velocities can be confined to above 400 km depth, and 2) velocities beneath about 800 km depth are those given by the Jeffreys-Bullen model. Each profile exhibits a gradual increase in velocity with depth, with discontinuities at 405 km and 659 km depth indicated by velocity increases of 4.5% and 7.5%, respectively.

The modeling of continental velocity structure has involved ten velocity profiles, four of which are shown in Figure 4. A standardized, 35-km-thick crust has been assumed for each structure and is listed in Table 2. Rays traveling upper mantle distances spend a proportionately small amount of their total traveltime within the crustal

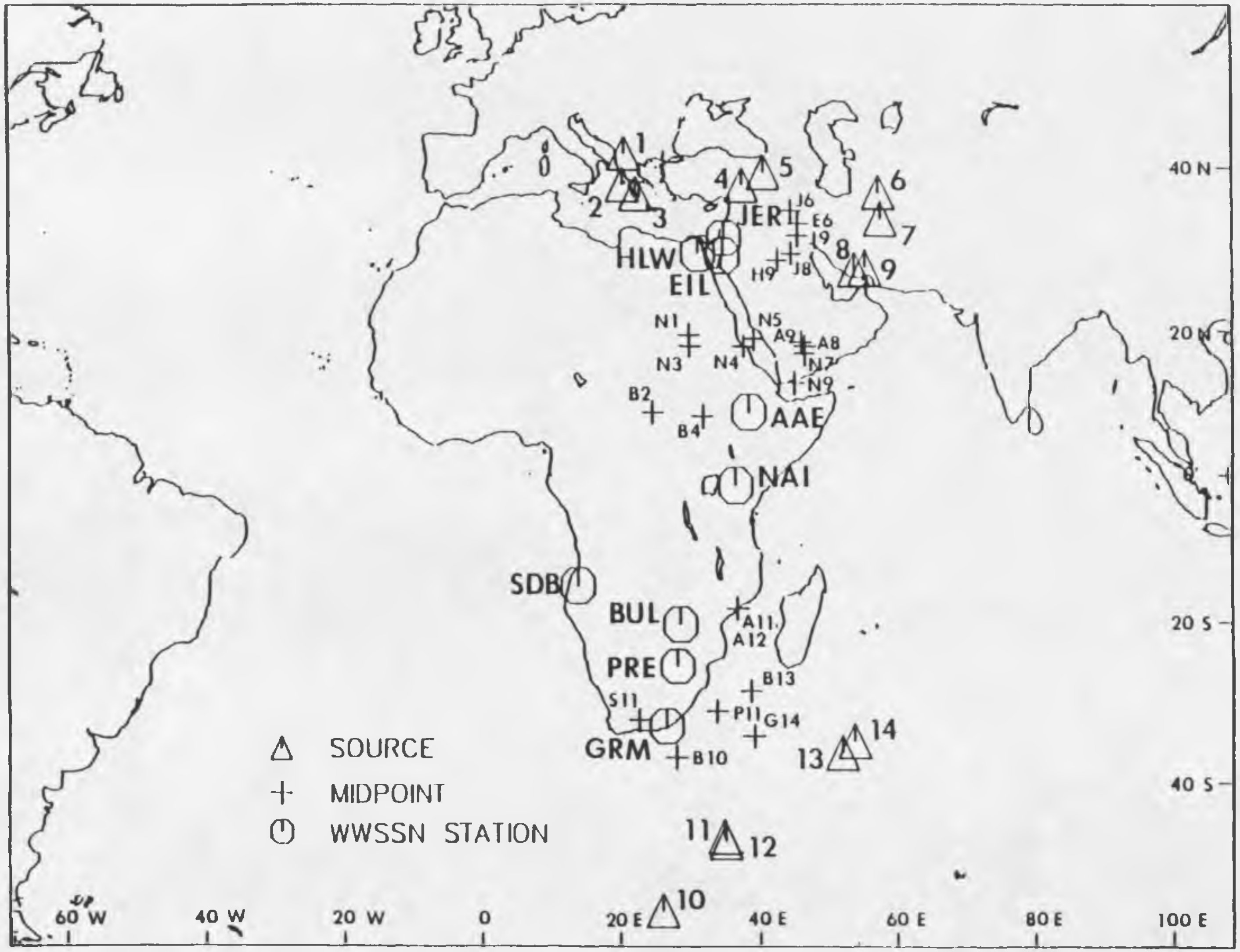


Figure 3. WWSSN stations, earthquake events, and raypaths used within this study of upper mantle shear velocity structure.

TABLE 1

LIST OF SEISMIC EVENTS

| Event | Date (mo/da/yr) | Lat (°N) | Long (°E) | Depth (km) | $m_b$ | Strike/Dip/Rake (degrees) | Reference |
|---|---|---|---|---|---|---|---|
| 01 | 11/30/67 | 41.50 | 20.50 | 29.0 | 6.0 | 157/50/-86.8 | a |
| 02 | 01/17/83 | 38.03 | 20.23 | 14.0 | 6.1 | 320/10/90[d] | b |
| 03 | 09/13/86 | 37.01 | 22.18 | 11.0 | 6.0 | 205/50/-68[d] | b |
| 04 | 05/05/86 | 37.99 | 37.80 | 5.0[e] | 5.9 | 352/67/177[d] | b |
| 05 | 08/20/66 | 39.42 | 40.98 | 5.0[f] | 5.3 | 13/76/194 | a |
| 06 | 01/03/69 | 37.13 | 57.90 | 11.0 | 5.6 | 132/60/85.5 | a |
| 07 | 09/01/68 | 34.04 | 58.22 | 15.0 | 5.9 | 148/65/64 | a |
| 08 | 09/18/66 | 27.90 | 54.30 | 18.0 | 5.9 | 270/34/96.6 | a |
| 09 | 06/21/65 | 28.10 | 55.90 | 40.0 | 6.0 | 102/34/63.5 | a |
| 10 | 09/91/83 | -52.48 | 25.84 | 20.0[g] | 5.3 | 320/82/-90[d] | b |
| 11 | 07/24/69 | -45.44 | 34.98 | 15.0[g] | 5.7 | 189/83/175 | c |
| 12 | 05/09/74 | -45.93 | 35.26 | 5.0 | 5.7 | 197/81/209 | c |
| 13 | 05/17/84 | -36.43 | 52.42 | 10.0 | 5.7 | 267/71/-4[h] | b |
| 14 | 12/24/85 | -35.09 | 54.27 | 10.0 | 6.0 | 95/87/0[d] | b |

[a]McKenzie, 1972.
[b]PDE (Preliminary Determination of Epicenters).
[c]Wald and Wallace, 1986.
[d]fault plane solution.
[e]depth decreased from 10.0 km.
[f]depth decreased from 12.0 km.
[g]depth increased from 10.0 km.
[h]moment tensor solution.

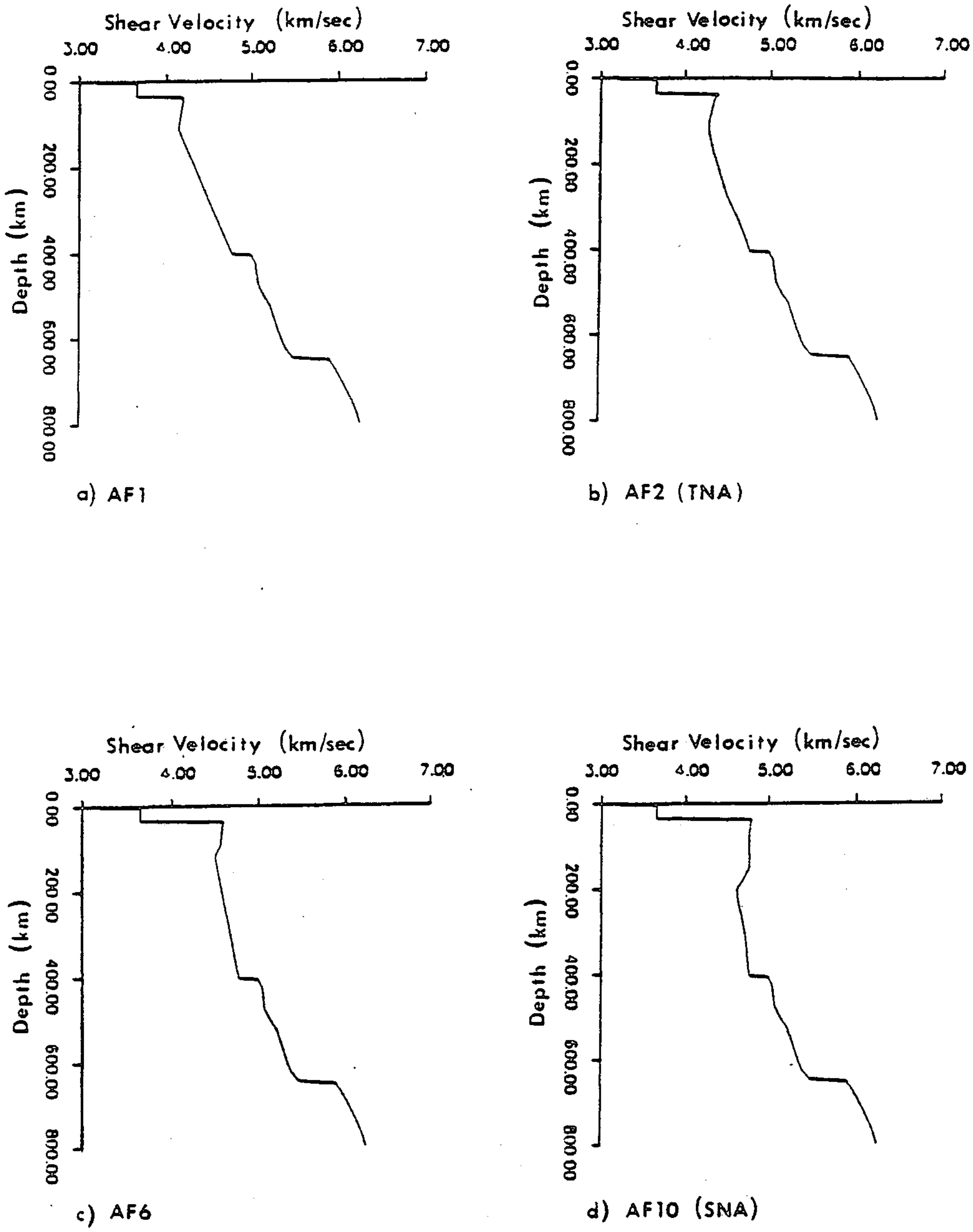


Figure 4. Four of the ten velocity profiles used to model continental shear velocity structure. These models demonstrate the progressive growth of a high velocity lid structure within the upper mantle. Included are Grand's (1986) models, TNA and SNA.

TABLE 2

CONTINENTAL CRUST

| Depth (km) | Shear Velocity (km/sec) |
|---|---|
| 0.0 | 3.20 |
| 3.5 | 3.20 |
| 4.0 | 3.65 |
| 35.0 | 3.65 |

structure. Therefore, although crustal structure is important, errors in the crustal approximation should not greatly affect the synthetic waveform. The series of velocity profiles in Figure 3 demonstrates both the progressive increase in upper mantle velocities and the growth of a high velocity lid structure to about 155 km depth. Included in the series are Grand's (1986) models for tectonic North America (TNA) and the stable Canadian shield (SNA).

The modeling of oceanic structure requires only two velocity profiles. These are shown in Figure 5. The first profile is identical to Grand's (1986) model for the Atlantic (ATL) while the second model is somewhat faster with a lid structure extending to 150 km depth rather than only 100 km depth. The crust is assumed to be 10 km thick with a velocity of 3.7 km/sec for both models.

Direct rays, with station-receiver separations of 15 to 27 degrees, are modeled assuming a laterally homogeneous structure for the entire raypath. In modeling SS waves, between 30 and 60 degrees, however, a laterally homogeneous structure is impractical as these raypaths typically extend across tectonic boundaries. Therefore, different velocity structures have been specified for source, midpoint, and receiver locations when necessary.

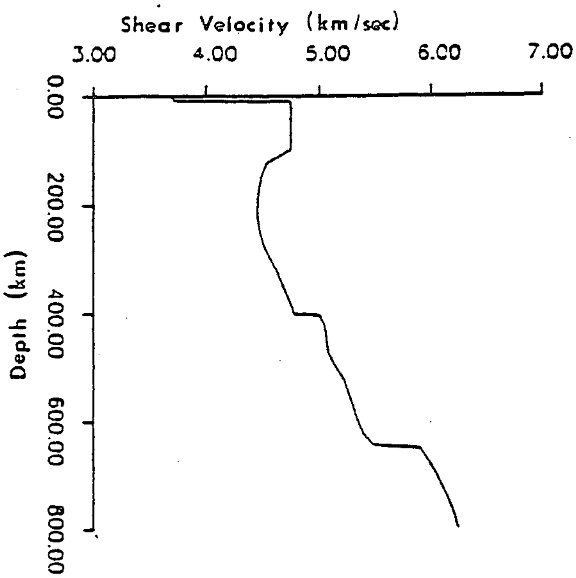


a) AF11 (ATL)

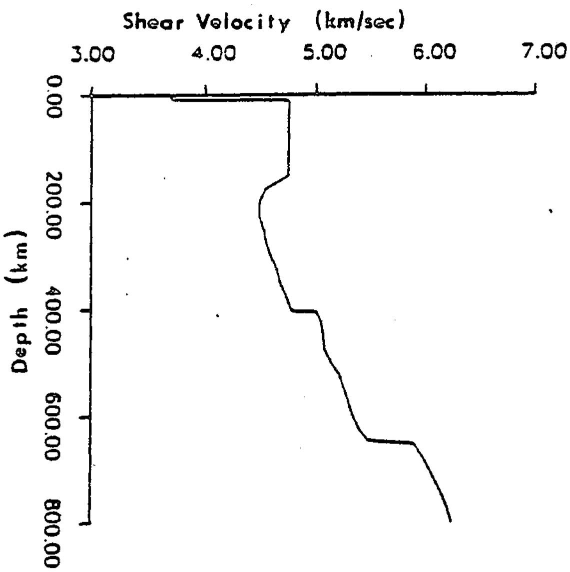


b) AF12

Figure 5. The two velocity profiles used to model upper mantle shear velocity structure beneath the Southwest Indian Ocean. Included is Grand's (1986) model, ATL.

# CHAPTER 5

# RESULTS

The upper mantle seismic velocity structure has been determined using a forward modeling technique. For each raypath this has involved the testing and modification of several velocity structures until the best waveform and traveltime fits were achieved. Two sets of traveltime data have been considered: 1) the absolute traveltimes associated with the S and SS phases, and 2) the SS-S time separation. A complete listing of traveltime errors associated with the synthetic seismograms is given in Table C.1, in Appendix C. Indicated by an asterisk is the one match which did not fall within the preferred traveltime constraint of 2.0 seconds (the S phase associated with raypath A6).

The locations of the 14 earthquakes and 22 raypaths, used within this study, are shown in Figure 2; the modeling results are listed in Table 3. While a summary of the upper mantle velocity distributions is given in this chapter, a more complete review of the modeling results is found in Appendix C. The vertical resolution of the shear velocity structure determined for each datapoint (source, midpoint, and receiver locations) is estimated at 100 km, the value of the average wavelength used within this study. This value has been calculated using the maximum observed shear velocity of 4.8 km/sec and an average period of 20 seconds. The radius of the first Fresnel zone, associated with plane incident waves, has been used to calculate a horizontal resolution of approximately 80 km (see Sheriff and Geldart, 1982). An average wavelength of 100 km and an average turning depth of 500 km are assumed in this calculation.

TABLE 3

LIST OF RAYPATHS

S DATA

| Raypath | Distance (degrees) | Model |
|---|---|---|
| E6 | 20.58 | AF4 |
| J6 | 19.45 | AF4 |
| A8 | 23.81 | AF6 |
| J8 | 17.02 | AF7 |
| A9 | 24.91 | AF6 |
| H9 | 21.55 | AF7 |
| J9 | 18.31 | AF5 |
| P11 | 20.39 | AF11 |
| B13 | 26.40 | AF12 |
| G14 | 22.95 | AF12 |

SS-S DATA

| Raypath | Distance (degrees) | Model |
|---|---|---|
| N1 | 45.07 | AFC1 |
| B2 | 58.39 | AFC2 |
| N3 | 40.44 | AFC1 |
| B4 | 58.47 | AFC3 |
| N4 | 39.08 | AFC4 |
| N5 | 40.68 | AFC4 |
| N7 | 40.49 | AFC5 |
| N9 | 34.49 | AFC6 |
| B10 | 32.35 | AFC7 |
| A11 | 54.32 | AFC8 |
| S11 | 35.37 | AFC9 |
| A12 | 54.80 | AFC8 |

Seismic rays which originate in Greece, Albania, or Turkey, and which travel towards northeast Africa, require a very slow upper mantle. Velocities are observed to decrease significantly as the rays approach or travel into the active rift zone. Seismic rays which travel beneath the Arabian peninsula, before entering northeast Africa, are affected by a similar decrease in velocities towards the rift zone. Unlike northeast Africa and the eastern Mediterranean, however, most of the Arabian shield requires a very fast upper mantle velocity structure. These high velocities are confined to the shield and give way rapidly to slower velocities towards the north (Iran, Iraq, and Syria) and towards the African continent.

Seismic rays originating from both northern and southern sources indicate an extremely fast upper mantle velocity structure beneath the South African craton, as well as beneath the easternmost extent of the West African craton. These regions have been modeled with the same high velocity structure that has been used by Grand (1986) for the stable Canadian shield. The transition from the East African Rift to the craton, as defined by seismic rays which traverse nearly the entire length of east Africa, occurs over a very narrow zone (<200 km). This suggests a relatively sharp upper mantle transition.

Relatively high velocities are indicated for the Southwest Indian Ocean, with the exception of a localized region near earthquake sources eight and eleven. The slow half-spreading rate of 1.0 cm/yr along the Southwest Indian Ocean Ridge (Bergh, 1971) has left relatively old oceanic material ($\geq$100 million years old) between the ridge system and the continent. Thus, very high upper mantle velocities are expected within this region. The isolated slower velocities may be attributed to a 'leaky transform'. This is consistent with the large component of dip-slip motion determined for several transform faults within the area (see Wald and Wallace, 1986).

In summary, rays traveling beneath southern Africa and the Arabian peninsula require less traveltime than those rays traveling comparable distances beneath northeast Africa. In general, seismic velocities are observed to decrease as rays approach the tectonically active rift zone. Lateral variations within the upper mantle seismic velocity structure decrease significantly with depth, such that all velocity profiles merge by about 400 km depth. More specifically, shear velocities beneath the African shield are approximately 14.25% higher at 125 km depth, 6.75% higher at 200 km depth, and only 3.5% higher at 300 km depth, as compared with velocities beneath the most active segments of the rift zone (Kenya and Ethiopia). Velocities beneath the eastern Mediterranean and the Arabian shield are intermediate between these two extremes.

Defining the base of the lithosphere as the base of the high velocity lid structure, lithospheric thickness has been mapped throughout the region of study (model LT1, Figure 6). Focusing on eastern Africa, seismic observations indicate (as have gravity data) that lithospheric thickness decreases, from west to east, from approximately 75 km to 40 km (or less). The thinnest lithosphere is found beneath those regions where young oceanic or intrusive material occurs along the rift floors. It is interesting that while the effects of rifting are evident throughout this wide zone within east Africa that significant lithospheric thinning is not apparent beneath the Arabian peninsula. Here, it is estimated that the lithosphere extends to a depth of about 125 km.

The estimates of lithospheric thickness beneath both the Caucasus and the northernmost extent of the Arabian plate are also of interest. A predominantly compressional regime exists throughout this region and thus a thickening of the continent might be expected. Yet, as is shown in model LT1, a relatively thin lithosphere, of only 75 km, is estimated. This thickens substantially to the south (near the northern border of Saudi Arabia) to about 125 km.

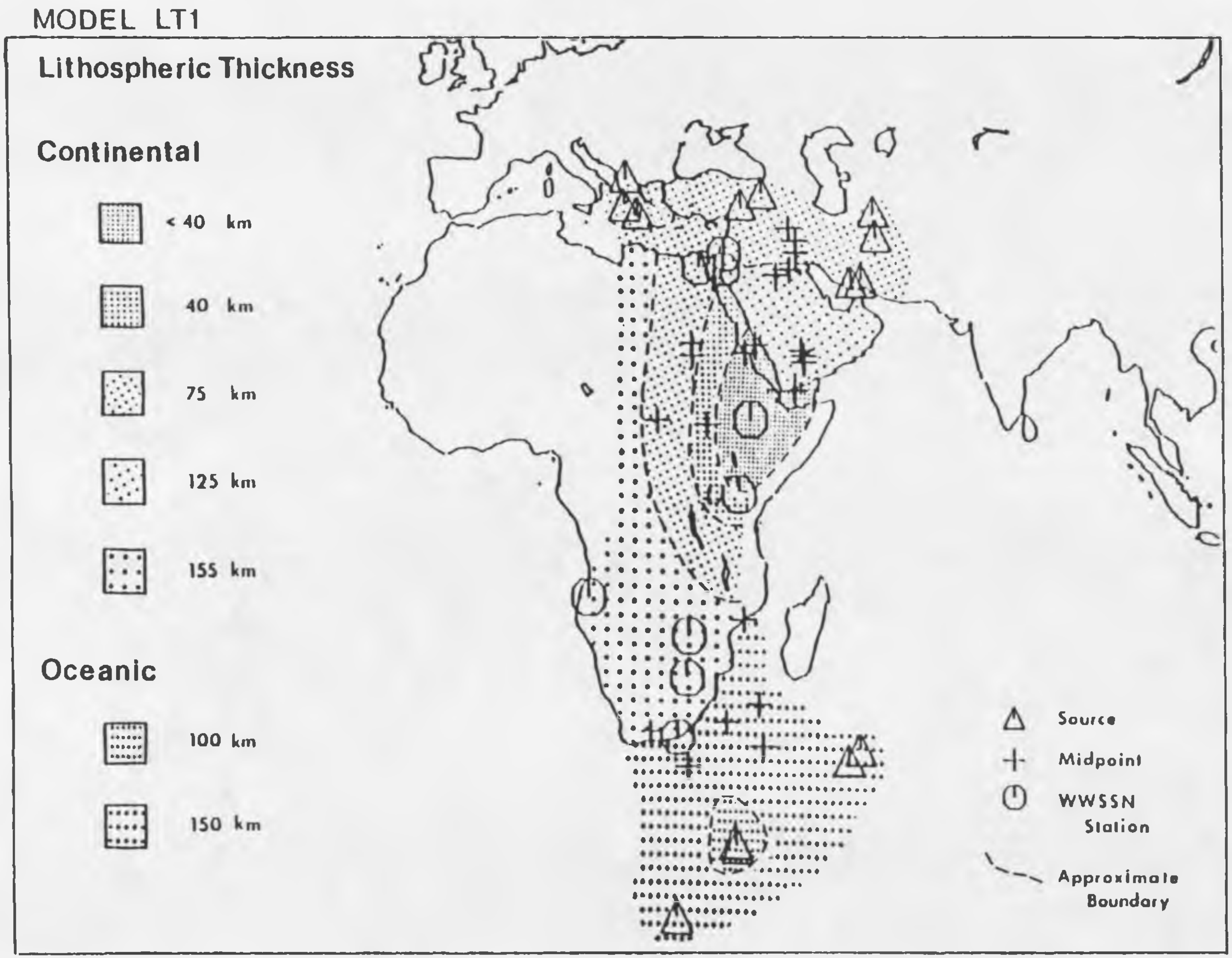


Figure 6. Model LT1.

The thickest lithosphere is found to the west and to the south of the East African Rift Zone and is estimated at about 155 km thickness. The upper mantle transition between this region and northeast Africa occurs over a very narrow zone (<200 km), in which the depth extent of the lithosphere decreases from 155 km to only 75 km. Within model LT1, this sharp transitional zone has been included within the boundaries of the 75-km-thick lithosphere. Although northwest Africa is not sampled by this study, research by others such as Burdick et al. (1983) and Grand et al. (1985) indicates that the thick lithospheric structure, found to the west and to the south of the rift zone, may extend beneath the West African craton as well.

The average lithospheric thickness beneath much of the Southwest Indian Ocean is estimated at 150 km. Although the depth extent of this oceanic lithosphere approaches that of the shield model, a much more extensive low velocity zone persists beneath the Southwest Indian Ocean than beneath the African shield regions. A somewhat thinner oceanic lithosphere, only 100 km thick, is indicated for the region surrounding earthquake sources eight and eleven.

# CHAPTER 6

## MODEL COMPARISONS

It is of interest to compare the models of shear velocity structure and lithospheric thickness, discussed in Chapter 4, with those derived through the use of other geophysical criteria. In 1984, Woodhouse and Dziewonski, using fundamental mode Rayleigh and Love waves as well as their first overtones, constructed global maps of upper mantle shear velocities, expanded to degree and order eight in spherical harmonics. This series of maps (given in 100-km-depth intervals between 50 and 550 km depth) indicates that the velocity anomalies associated with shields and oceanic ridge systems are apparent to at least 250 km depth, with the larger shields exhibiting faster than normal velocities to 350 km depth or more. The scale of the shear velocity heterogeneity decreases from approximately $\pm$ 8% at 50 km to $\pm$ 2.5% at a depth of 450 km. Below 450 km depth, however, very little correlation is apparent between the upper mantle velocities and the surface tectonic features. Lateral resolution throughout this series is on the order of 2000 km.

The distribution of upper mantle shear velocities indicated by Woodhouse and Dziewonski is very similar to the distribution of velocities determined in this study using long-period bodywaves. Both models associate anomalously high shear velocities with the African shield to a depth of at least 400 km, as compared with the velocity structure beneath the eastern Mediterranean and the active rift zone of northeast Africa. The most apparent difference between the two models, however, involves the interpretation of the velocity structure beneath the Arabian peninsula. Woodhouse and

Dziewonski designate this region as a low velocity feature beneath about 200 or 250 km depth, whereas seismic observations used in this study indicate relatively high velocities to at least 400 km depth. This discrepancy may be attributable to the limited lateral resolution (2000 km) of the Woodhouse and Dziewonski (1984) study.

A vastly different approach to studying the upper mantle structure is used by Pollack and Chapman (1977), in which higher order harmonics are used to predict lithospheric thickness from regional variations in surface heat flow. Families of continental and oceanic geotherms are produced from a twelfth degree spherical harmonic representation of global heat flow (see Chapman and Pollack, 1975). The depth at which these geotherms reach 0.85 of the melting temperature is considered an approximation of the depth to the top of the low velocity zone (or the base of the high velocity lid structure). Defining the base of the lid structure as the base of the lithosphere, Pollack and Chapman predict that lithospheric thickness ranges from just a few tens of kilometers beneath young oceanic and tectonically active regions to greater than 300 km beneath shield regions. It should be noted, however, that heat flow measurements were obtained for approximately only 42% of the Earth's surface area and that heat flow values were estimated for the remaining regions based on known geologic and tectonic information (Pollack and Chapman, 1977). This lack of observed data should be considered when reviewing the modeling results.

Although general agreement does exist between this model (based upon surface heat flow) and model LT1, significant differences are apparent. Within southern Africa, model LT1 indicates a lithospheric thickness of approximately 155 km. This value is bracketed by Pollack and Chapman's estimates of 100 to 200 km. In northeast Africa, both models suggest lithospheric thinning towards the Afar triple junction. The extent of the lithospheric thinning, however, is much greater in model LT1. For example, near the Afar triple junction, a lithospheric thickness of only 40 km (or less) is indicated by model LT1. In contrast, Pollack and Chapman propose a lithospheric thickness of 60 km. Similarly, Pollack and Chapman predict a somewhat thicker lithosphere (100-125 km) for both the Caucasus and the region extending from the easternmost Mediterranean to western Iran, than that which is indicated in model LT1 (75 km). The greatest discrepancy, however, concerns the Arabian shield. Pollack and Chapman predict that lithospheric thickness beneath the Arabian shield is very similar to that beneath the East African Rift, 60 to 75 km. In contrast, this study indicates a lithospheric thickness of approximately 125 km for the Arabian shield, which is significantly greater than the range of lithospheric thicknesses ($\leq$40 to 75 km) estimated for the active rift zone. Although several discrepancies between the Pollack and Chapman (1977) model and model LT1 are noted above, it is probable that these differences (in part) are related to the limited coverage of heat flow data used by Pollack and Chapman (1975) to produce the global map of heat flow from which geotherms and lithospheric thickness were determined. In addition, surface heat flow values can lag by tens of millions of years in achieving thermal equilibrium with the base of the lithosphere.

# CHAPTER 7

## IMPLICATIONS FOR PLATE TECTONICS

A significant number of seismological studies, throughout the past decade or so, have provided evidence for a rather consistent correlation between upper mantle shear velocity structure and thermotectonic history (e.g., Sipkin and Jordan, 1975, 1976; Woodhouse and Dziewonski, 1984; Grand, 1986). In particular, a relatively fast sub-shield mantle, as compared with velocities beneath young oceanic and tectonically active provinces, has been postulated. The depth extent and the nature of the lateral heterogeneity, however, remain somewhat controversial. Several models have been proposed to explain these variations in seismic structure. While deciding among these is not the purpose of this paper, a review of two models, Jordan (1975, 1978) and Anderson (1987), is given with the intent of examining implications for global plate tectonics and chemical and thermal evolution of the Earth's upper mantle.

Jordan (1975, 1978) proposes that lateral contrasts in compositional and thermal structure, extending deep into the upper mantle, are responsible for the lateral variations observed in the shear velocity structure. He argues that the high velocity root zones situated beneath continental shields extend to about 400 km depth (or greater). These root zones are included in that portion of the upper mantle structure referred to as the tectosphere. The tectosphere is defined as a thermal boundary layer which translates coherently as a single vertical unit during horizontal plate motions (Jordan, 1975). Beneath young oceanic and tectonically active regions the tectosphere is a very thin layer, typically less than 100 km thick. Beneath shield regions, however, the tectosphere may extend to depths greater than 400 km and is characterized by relatively low temperatures and high seismic velocities, a superadiabatic thermal gradient, and a distinct basalt-depleted chemical composition.

Geotherms constructed for both oceanic and continental provinces (see Jordan, 1975, for a detailed discussion) are used to demonstrate lateral heterogeneity within the upper mantle thermal structure. Temperature gradients indicate that old oceanic material (100 million years old) is underlain by a conductive layer to about 150 km depth. Temperatures at greater depth, however, follow a 1300°C adiabat (Jordan, 1975). In contrast, subshield temperatures are much lower. The subshield geotherm does not merge with the oceanic geotherm (1300°C adiabat) until at least 400 km depth (Jordan, 1975), resulting in superadiabatic temperature gradients beneath the continental shields.

The occurrence of superadiabatic thermal gradients within the continental root zones presents at least two problems. First, it is necessary to explain why convective flow has not been induced by the superadiabatic gradients. Second, the cooling of upper mantle material to a depth of 400 km should be accompanied by a significant increase in density and thus notable subsidence. This has not been observed. Both problems are eliminated by introducing a compositional gradient in which the subshield chemical composition is less dense that that of the surrounding upper mantle. More specifically, Jordan suggests a basalt-depleted chemical root, for subshield mantle, to about 400 km depth. Not only should such a compositional gradient guard against the onset of convection, but the density increase associated with the cooling of upper mantle material should be approximately balanced by the density decrease associated with basalt-depletion.

Jordan (1975, 1978), therefore, maintains that lateral contrasts within the shear velocity structure extend to at least 400 km depth. He proposes that the high velocity root zones situated beneath continental cratons are the result of large lateral variations in thermal and chemical structure, also extending to about 400 km depth.

Anderson (1987) agrees that lateral variations within the upper mantle seismic velocity structure can be correlated with tectonic history to a depth of at least 400 km. He argues, however, that thick conductive roots, with large lateral variations in temperature and chemical composition, are not necessary to explain the high seismic velocities indicated for subshield mantle. Rather, he suggests that while chemical roots may extend to a depth of about 150 km, the velocity structure between 150 and 400 km depth can be readily explained by adiabatic compression along a 1400°C adiabat (Anderson and Bass, 1984). Furthermore, Anderson (1987) claims that the slower velocities associated with the upper mantle structure of oceanic and tectonically active provinces can be attributed to thermally induced isobaric phase changes, such as partial melting, which require only slight temperature increases along the shield adiabat.

Several studies have shown that continental plates, in general, move more slowly than do oceanic plates. For example, using a hot spot reference frame, Minster et al. (1974) determined the average velocity for oceanic plates to be approximately five times greater than that for continental plates. As a result, many studies have assumed an increase in viscous drag beneath the continents (Minster et al., 1974; Solomon and Sleep, 1974) and in particular beneath the shield regions (Pollack and Chapman, 1977) and have suggested that the existence of thick conductive roots, as proposed by Jordan (1975, 1978), should have important implications for global plate tectonics. The viscous coupling, between the base of the tectosphere and the underlying mantle material, should be expected to increase significantly with the progressive growth of a continental root zone. This should create a 'viscous anchor' which will serve to gradually decrease horizontal plate motion (Pollack and Chapman, 1977). Such a situation has been postulated by Chapman and Pollack (1974) for the West African shield to explain the apparent lack of motion of the African plate (with respect to hot spots) for the past 25 million years (Burke and Wilson, 1972; Sengor and Burke, 1978). It has been predicted that as viscous coupling continues to increase beneath the shield regions, a greater number of continental plates will become 'anchored', and thus all plate motion may come to an eventual end (Pollack and Chapman 1977).

The concept of 'viscous anchors', however, is questionable and is not necessarily consistent with other geologic and geophysical observations. As an example, due to the high basal shear stresses indicated for the 'viscous anchor' a net torque on the lithospheric plate would be expected for any horizontal plate motion. This phenomenon has not been observed. In addition, analyses of global plate motions indicate that the present-day slow velocities observed for predominantly continental plates are not representative of continental plate motions throughout all time. Evidence exists that major continental plates have, in the past, moved at velocities much greater than velocities observed today (Solomon et al., 1977; Gordon et al., 1979; Jurdy and Gordon, 1984; Gordon and Jurdy, 1986). In particular, the results of Gordon et al. (1979) show that while continental plates (with the exception of the Indian plate) have consistently moved slower than oceanic plates throughout the past 350 million years, continents have at times moved much more rapidly than present continental plates for intervals of time extending approximately 30 million years in length. A study by Solomon et al. (1977) indicates absolute velocities of certain continental plates during the early Tertiary actually exceeded the absolute velocities of oceanic plates. The results of this study, however, are the subject of much controversy (see Gordon et al., 1978; Jurdy, 1978; Jurdy and Gordon, 1984). Consistent with the determination of variable plate velocities throughout time driving force models should not require significant increase in viscous drag beneath continental areas. While many studies indicate drag forces associated with continental plates are larger than those associated with oceanic plates (e.g., Solomon and Sleep, 1974; Forsyth and Uyeda, 1975; Richardson et al., 1979; Gordon and Jurdy, 1986), viscous drag in all cases is relatively small (as compared to other forces acting on the plate) and cannot be the dominant force controlling plate motions (Forsyth and Uyeda, 1975; Richardson et al. 1979). Gordon et al. (1979) suggest the relatively slow continental plate velocities observed today are an 'accident' of the current arrangement of lithospheric plates.

Forsyth and Uyeda (1975) find a strong positive correlation between absolute plate velocity and the percentage of the plate attached to subducting slab. For instance, lithospheric plates which are predominantly oceanic and which have a large percentage of their boundaries connected to downgoing slabs (such as the Pacific, Cocos, and Nazca plates) exhibit absolute velocities of 6 to 9 cm/yr, wheareas plates not connected to slabs (such as the Eurasian, North American, and African plates) exhibit velocities of only 0 to 4 cm/yr (Forsyth and Uyeda, 1975). Forsyth and Uyeda (1975) suggest the negative buoyancy force pulling the slab downward is nearly balanced by a resistive force encountered at approximately the asthenosphere-mesosphere boundary (consistent with a significant increase in mantle viscosity). The resultant net force (slab pull plus slab resistance) acts to pull the attached plate toward the zone of subduction. Currently, no major continental plates are being actively subducted. This factor has apparently contributed to the slower velocities observed for continental plates (Gordon et al., 1979). A study of intraplate stress fields by Richardson et al. (1979) provides a further test of the relative importance of various driving forces for global plate tectonics. Comparisons of the observed stress orientations with those predicted for the different driving force models indicate that ridge push force (resulting from the elevated topography of the mid-oceanic ridges) may be as significant in controlling lithospheric plate deformation as the balance of forces acting on the downgoing slab (Richardson et al., 1979). Additional forces acting at plate boundaries, such as the pull of overthrust (or continental) lithosphere towards the subduction zone may also be of some significance (Elsasser, 1971; Chase, 1978).

If it can be assumed that global plate motions are affected primarily by the forces acting on plate boundaries (such as ridge push, slab pull, and slab resistance) then the distribution of absolute plate velocities determined for any time interval should be directly related to the plate geometries existing at that time and the percentage of plate boundaries occupied by active subduction zones and oceanic ridge systems. The velocity of the African plate relative to the underlying mantle material can, therefore, be explained without appealing to a substantial increase in viscous drag beneath the West African shield.

## CHAPTER 8

## DISCUSSION AND CONCLUSIONS

One of the primary purposes of this study has been to examine the relation between lateral heterogeneity within the upper mantle shear velocity structure and surface tectonic features. In the past, most studies of the upper mantle velocity structure have concentrated on surface wave dispersion. Although this research has been valuable in providing average velocity variations on a global scale, detailed resolution has not been possible due to the required use of relatively long-period data. A second approach, which offers finer resolution of structural detail, has involved the measurement of bodywave traveltimes. In particular, velocity models have been constructed by measuring traveltime anomalies for both primary and secondary arrivals and by comparing traveltime curves for various tectonic regimes. More recently, these models of upper mantle velocity structure have been further constrained through the use of synthetic seismogram modeling. In the forward modeling problem, an initial velocity structure is tested by comparing the synthetic waveform with the observed seismic data. The model is then adjusted, if necessary, until the discrepancies between the observed and synthetic seismograms are minimized.

Numerous surface wave and bodywave studies have provided evidence for lateral heterogeneity within the upper mantle seismic velocity structure. Still somewhat controversial, however, are the scale and depth extent of this heterogeneity, as well as the relation between upper mantle velocities and thermotectonic history. In this thesis the tectonic signature on the upper mantle shear velocity structure has been investigated for a region of extreme lateral tectonic heterogeneity. More specifically, forward modeling of long-period S and SS waveforms has been used to examine the upper mantle transition from the tectonically active East African Rift Zone to the adjacent shield regions of west Africa, south Africa, and the Arabian peninsula. Of particular concern was whether traveltime and waveform differences could be mapped into the velocity structure at depths shallower than 400 km.

This study has found significant differences in upper mantle shear velocity structure which can be directly correlated with the thermotectonic history of the African plate and the surrounding region. Seismic rays which propagate beneath the eastern Mediterranean and much of northeast Africa require relatively slow upper mantle velocities and are modeled with a very thin lid structure of approximately 75 km thickness. Upper mantle velocities and lid thickness are observed to decrease substantially as the seismic rays approach the East African Rift Zone. As a result, the high velocity lid structure is completely absent beneath the more active portions of the rift system. In contrast, the shield regions of west Africa and south Africa are modeled with anomalously high upper mantle velocities to about 400 km depth. The shear velocity structure indicated for these shield regions includes a prominent lid structure to about 155 km depth overlying a well-developed, but very thin, low velocity zone. This same structure has been used by Grand (1986) for the tectonically stable Canadian shield of the North American plate. The upper mantle shear velocities of the Arabian shield, while similar, are slightly slower and correspond to a somewhat thinnner lid structure.

Defining the base of the lithosphere as the base of the high velocity lid structure, a regional map of lithospheric thickness has been constructed for the region of study. The thinnest lithosphere is located beneath those regions where young oceanic or intrusive material occurs along the rift floors (the Kenyan and Ethiopian rift segments, the Red Sea, and the Gulf of Aden). In general, lithospheric thickness increases with distance from the rift zone, reaching maximum values of 125 km beneath the Arabian shield and 155 km beneath the West African and South African shields.

The upper mantle transition from the tectonically active East African Rift Zone to the surrounding stable craton, studied in this paper, is represented by the progressive development of a high velocity lid structure to about 155 km depth and an overall increase in upper mantle velocities to about 400 km depth. A systematic relation exists between thermotectonic history and upper mantle velocity structure, such that regions of recent extensional tectonic activity have relatively slow velocities to about 400 km depth. It has been shown that seismic velocities from differing tectonic regimes are consistent with velocity models which merge by approximately 400 km depth, indicating very little lateral variation in the upper mantle seismic velocity structure beneath this depth.

## APPENDIX A

## NONUNIQUENESS OF FORWARD MODELING RESULTS

The distribution of upper mantle seismic velocities, determined for this region of study, is the result of forward modeling of long-period bodywaves. For each raypath this has involved the testing and modification of several velocity structures until the best waveform and traveltime fits were achieved. This technique has provided an acceptable representation of the velocity structure, but not necessarily a unique representation. This is illustrated in Figure A.1. Figure A.1 includes three velocity profiles which are identical except for the placement of the 100-km-thick low velocity zone. This zone is encountered at 100 km, 150 km, and 200 km depth for models M1, M2, and M3, respectively. Also shown in Figure A.1 are synthetic waveforms corresponding to each velocity structure at distances of 17, 19, and 21 degrees. These have been arranged such that the synthetic seismograms, constructed for the three velocity profiles at a given distance, can be readily compared. A review of the seismograms, at any of the three distances, shows that waveforms and traveltimes are remarkably similar. The slight differences which do exist, might easily fall within the limits of acceptable data for many studies.

It is shown that as the low velocity zone increases in depth (from left to right in Figure A.1) rays turning above the 405 km discontinuity (first peak) require progressively greater traveltime. Traveltimes of rays from below and at the discontinuity (second and third peaks), however, are not altered by more than 0.6 seconds. Therefore, from left to right, the separation of the first two arrivals is progressively

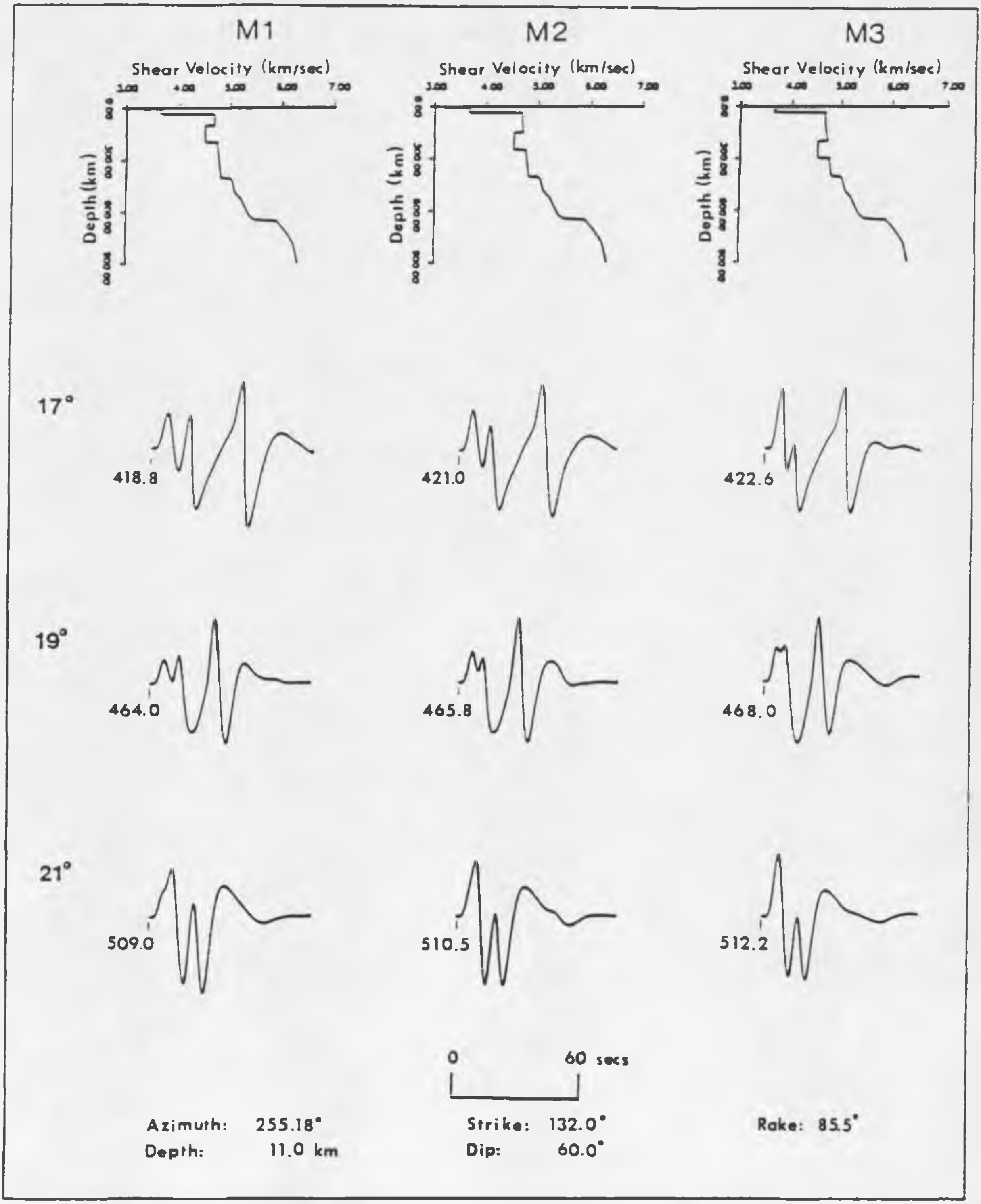


Figure A.1. A comparison of the synthetic waveforms and traveltimes for models M1, M2, and M3. The three velocity models are identical except for the placement of the low velocity zone.

decreased. Seismic rays traveling through velocity structure M3 are closer to triplication than are rays traveling through velocity structure M1 (for any given distance). These changes are reflected in the traveltime curves. In particular, the branch corresponding to rays turning above 405 km depth (branch A) should become progressively steeper as the low velocity zone is placed deeper in the structure. As a result, the separation between this branch and the branch representing rays turning below the discontinuity (branch B) should be slightly decreased. The separation of rays turning below and at the 405 km discontinuity (branch C), however, remains essentially constant. An example of this is shown in Figure A.2.

Based upon the above discussion, upper mantle velocities determined from the modeling of a single raypath or from several isolated raypaths should be viewed with skepticism. This study, however, uses a multiplicity of raypaths and in particular includes a number of raypaths which either parallel or intersect each other. As a result, the distribution of upper mantle velocities indicated by this study are relatively well constrained, although nonuniqueness of the model cannot be completely eliminated.

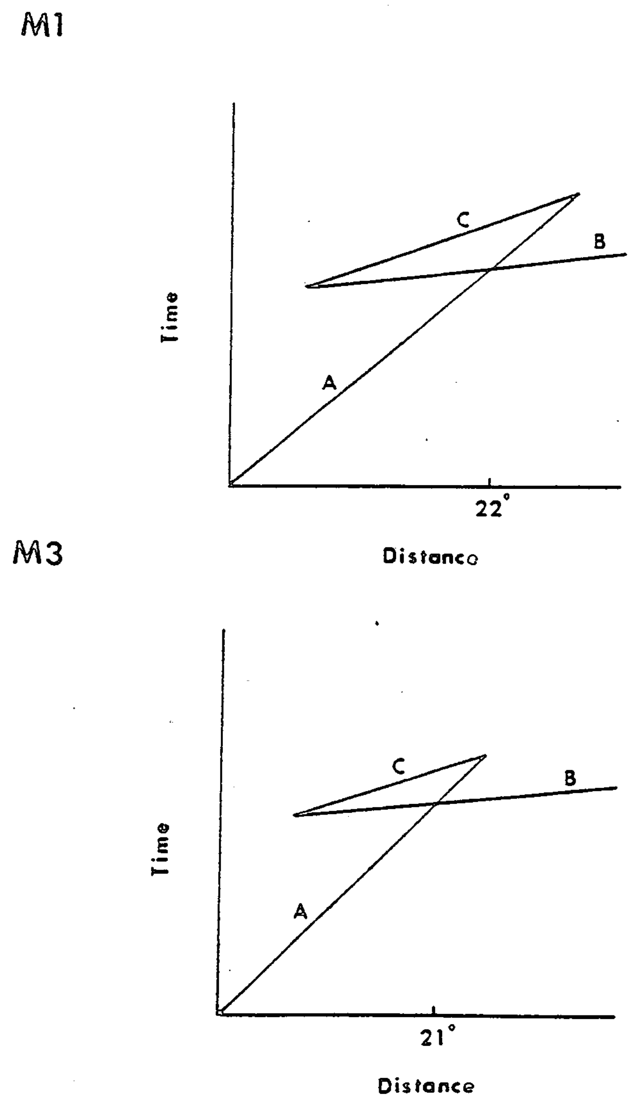


Figure A.2. A schematic illustration of traveltime curves for models M1 and M3.

## APPENDIX B

## INTERPRETATION OF THE SYNTHETIC SEISMOGRAM

The use of synthetic seismogram modeling has resulted in an increased understanding of the seismic waveform. For example, changes in the waveform can be studied as different modeling parameters are varied. Figure B.1 shows predicted changes in waveform related to changes in velocity structure and source-receiver distances. Synthetic waveforms have been computed at distances of 17 to 23 degrees for nine of the ten continental velocity structures used within this study. An almost pure thrust fault is assumed for the earthquake source.

Synthetic seismograms are also useful in understanding the sequence in which seismic rays are received at a particular station. For example, the seismogram constructed for velocity structure AF8 at 17 degrees includes three peaks, corresponding to seismic rays which turn above, below, and at the 405 km discontinuity, respectively. These three rays arrive closer and closer together, until finally at 21 degrees the two rays from above and below the discontinuity arrive simultaneously (triplication point). At distances just beyond this, the ray turning below 405 km depth requires the least amount of traveltime and is the first ray to arrive at the station. Beyond triplication, however, as the source-receiver distance is increased, all seismic arrivals are very close together in time. As a result, the waveform does not appear to change significantly at these greater distances. It is therefore very difficult, by visual analysis of the waveform alone, to interpret the second point of triplication, when rays turning above and below the 659 km discontinuity arrive simultaneously.

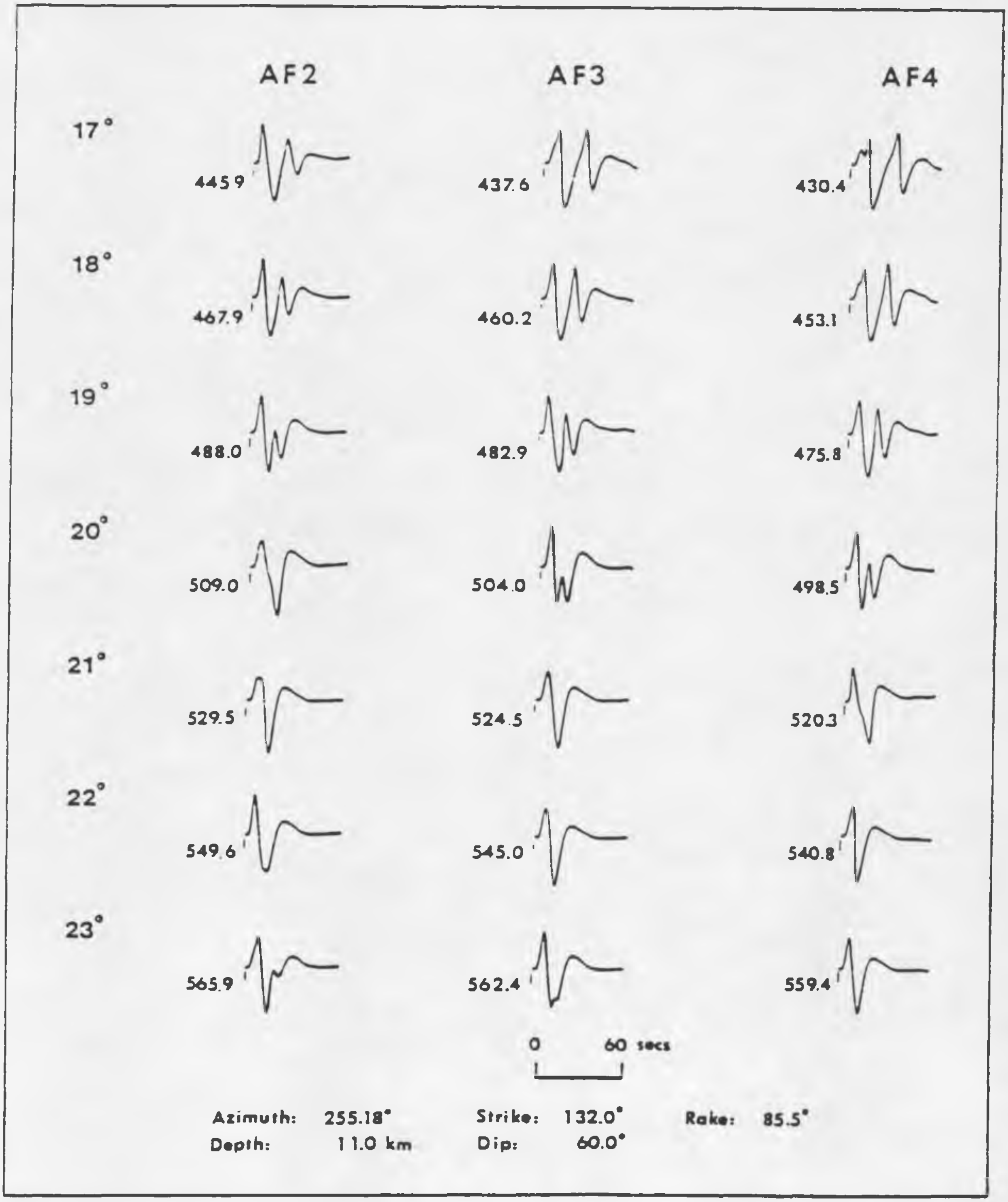


Figure B.1(a). Synthetic seismograms computed for continental velocity models AF2, AF3, and AF4 for the distance range of 17 to 23 degrees. These synthetics illustrate progressive changes in waveform and traveltime associated with variations in distance and lid structure.

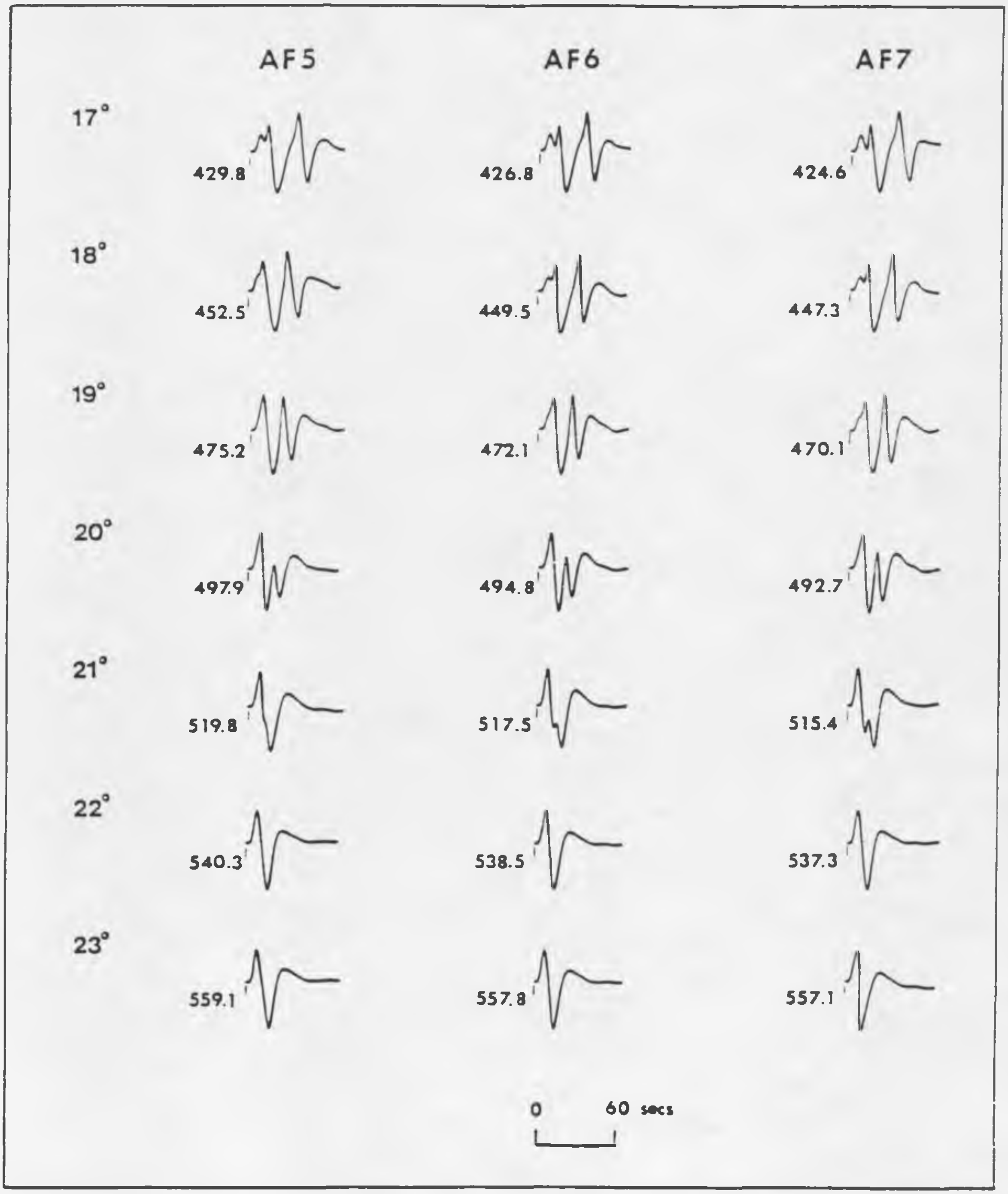


Figure B.1(b). Synthetic seismograms computed for continental velocity models AF5, AF6, and AF7 for the distance range of 17 to 23 degrees. These synthetics illustrate progressive changes in waveform and traveltime associated with variations in distance and lid structure.

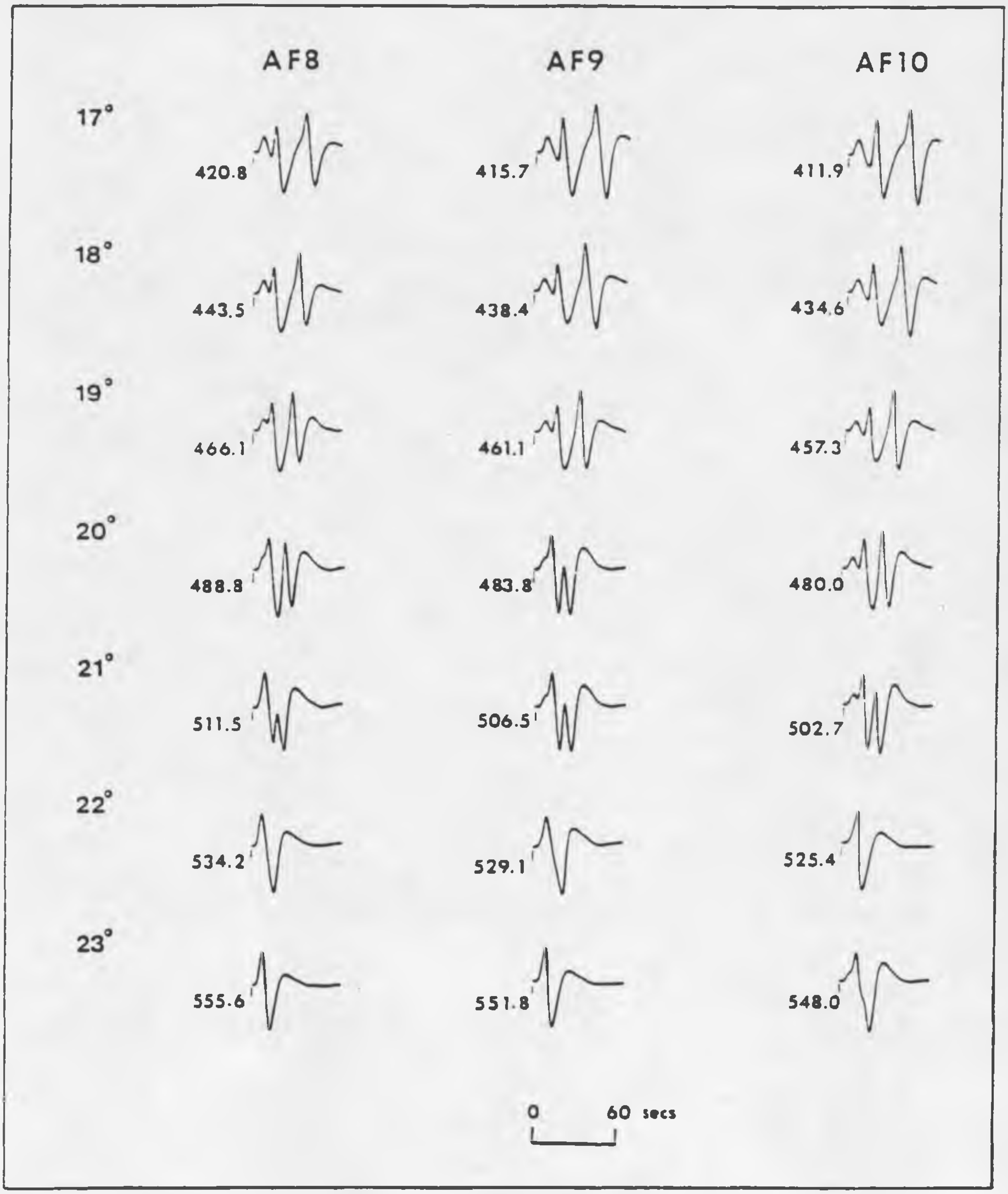


Figure B.1(c). Synthetic seismograms computed for continental velocity models AF8, AF9, and AF10 for the distance range of 17 to 23 degrees. These synthetics illustrate progressive changes in waveform and traveltime associated with variations in distance and lid structure.

Reviewing the waveforms in Figure B.1, it is apparent that triplication does not occur at the same distance for each velocity structure. Rather as velocities and lid thickness increase (as shown from left to right in Figure B.1) the distance at which triplication occurs also increases. For example, the triplication, resulting from the 405 km discontinuity, is observed at about 17 degrees for model AF2 but not until about 23 degrees for model AF10. Table B.1 lists the approximate distance at which triplication occurs for each velocity structure.

Three trends related to an increase in source-receiver distance, while the velocity structure remains constant, are:

1) traveltimes increase due to rays traveling further distances
2) turning depths of individual seismic rays increase, and
3) the length of the wavetrain decreases due to seismic rays arriving closer and closer together as the point of triplication is approached.

Three trends related to an increase in upper mantle velocities and lid thickness, while the distance remains constant, are:

1) traveltimes decrease due to rays traveling through faster velocity structures,
2) turning depths associated with individual rays decrease, and
3) triplications occur at increased distances. This produces waveforms which are more complicated and which are increased in length due to seismic rays arriving further apart in time.

Varying the depth of the earthquake source provides an additional change in the synthetic waveform. An increased source depth results in a greater S-sS traveltime separation and thus a slightly more complex waveform. An example of this is illustrated in Figure B.2 using a source-receiver distance of 39.08 degrees and an almost pure

TABLE B.1

TRIPLICATION DISTANCES*

| Model | Triplication (degrees) |
|---|---|
| AF1 | <17.0 |
| AF2 | 17.0 |
| AF3 | 18.0 |
| AF4 | 18.5 |
| AF5 | 19.0 |
| AF6 | 19.5 |
| AF7 | 20.0 |
| AF8 | 21.0 |
| AF9 | 22.0 |
| AF10 | 23.0 |

*Triplication distances correspond to the 405 km discontinuity.

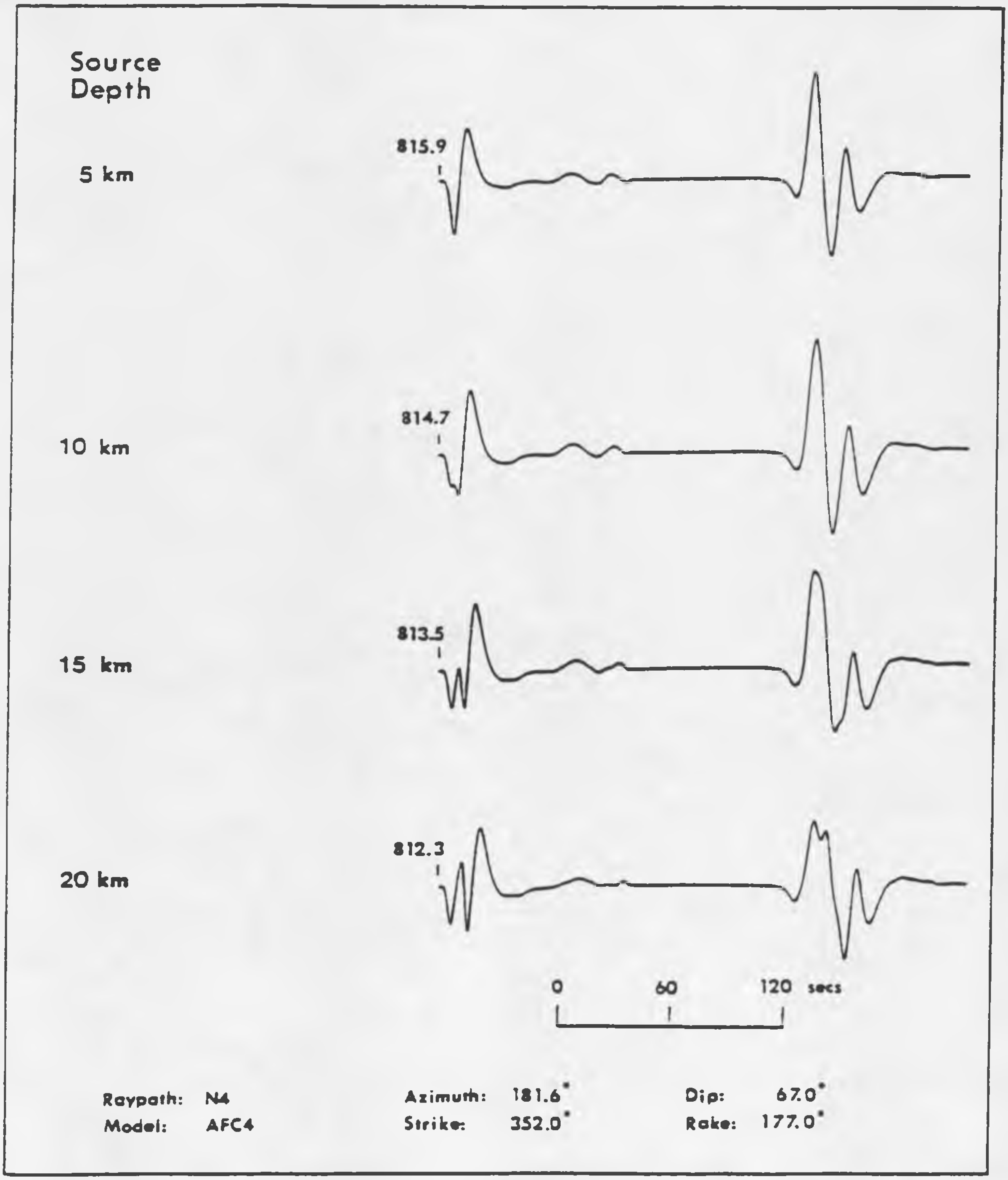


Figure B.2. A comparison of synthetic seismograms computed for different source depths.

left-lateral strike-slip fault with a dip of 67.0 degrees. As the source depth is increased, in 5-km intervals between 5 and 15 km, the S wave (which travels downward from the source) requires progressively less traveltime. In contrast, the sS wave (which travels upward from the source before being reflected at the surface) must travel a slightly greater distance and, therefore, requires increased traveltime. In figure B.2, the S and sS phases are shown to coincide when a source depth of 5 km is used. The separation between these two phases, however, is observed to increase as the source depth is increased. Similarly, the interaction between the SS and sSS phases also changes as the source depth is varied.

## APPENDIX C

## MODELING RESULTS

The distribution of upper mantle seismic velocities discussed in this section for east Africa, the Arabian shield and the eastern Mediterranean is the result of forward modeling of long-period S and SS waveforms. Vertical shear velocity profiles have been determined to about 800 km depth with significant lateral variations confined to above 400 km depth. The 14 earthquakes and 22 raypaths used in this study are shown in Figure 3 of the main text. Seismic events and raypaths are listed in Tables 1 and 2, respectively. Direct rays with station-receiver separations of 15 to 27 degrees, are modeled assuming a laterally homogeneous structure for the entire raypath. This is not a practical assumption, however, for SS waves (30 to 60 degrees) as these raypaths typically extend across tectonic boundaries. Therefore, different velocity structures have been specified for source, midpoint, and receiver locations when necessary.

Rays traveling from northern sources (Greece, Albania, Turkey, and Iran) into the African continent provide information on velocity gradients beneath northeast Africa, the eastern Mediterranean, and the Arabian shield. Likewise, rays traveling from southern sources (along the Southwest Indian Ocean Ridge system) are valuable in constraining the upper mantle shear velocity structure beneath southern Africa.

Following is a detailed review of each raypath and the velocity structure through which it passes. The discussion begins with SS rays which travel predominantly beneath either northeast Africa or the Arabian shield. This is followed by a review of the northern S data in which rays travel either directly beneath or just north (along east-west paths) of the Arabian shield. SS rays traveling nearly the entire length of the continent (from north to south) are discussed, providing information on both northern and southern east Africa as well as the transition between the East African Rift and the craton. Finally, S waves traveling between the Southwest Indian Ocean Ridge and the continent, as well as SS waves traveling into southern Africa, are reviewed. In each of the following figures which compares synthetic and observed seismograms, the synthetic waveform is placed below the observed waveform.

## Raypaths N1 and N3

The two westernmost raypaths shown in Figure C.1, N1 and N3, are modeled with source, midpoint, and receiver velocity structures AF4, AF3, and AF1, respectively, as is shown in model AFC1 (Figure C.2). This particular sequence of velocity profiles indicates a decrease in velocities from source to midpoint to receiver, as might be expected for rays traveling towards and then into an active rift zone. The two earthquake sources, located in a region of present-day extensional tectonics, have been modeled with a relatively slow velocity structure, corresponding to a very thin lid of approximately 75 km. The two rays are reflected beneath the country of Sudan in northeastern Africa. Midpoint velocities are those given by velocity profile AF3. Although these midpoint velocities may at first seem slow, considering the distance from the rift activity, substituting the faster velocity profile AF4 results in SS phases arriving 5.0 to 6.0 seconds early. As should be expected, substituting the slower velocity structure, AF2, results in SS arriving 3.5 to 8.0 seconds late. Model AF3, therefore, seems an appropriate estimate of the midpoint velocity structure. Seismic station NAI has been modeled with the slowest velocity structure available, AF1, showing no indication of a high velocity lid. This is not surprising considering Nairobi, Kenya, is one of the more active portions of the rift zone.

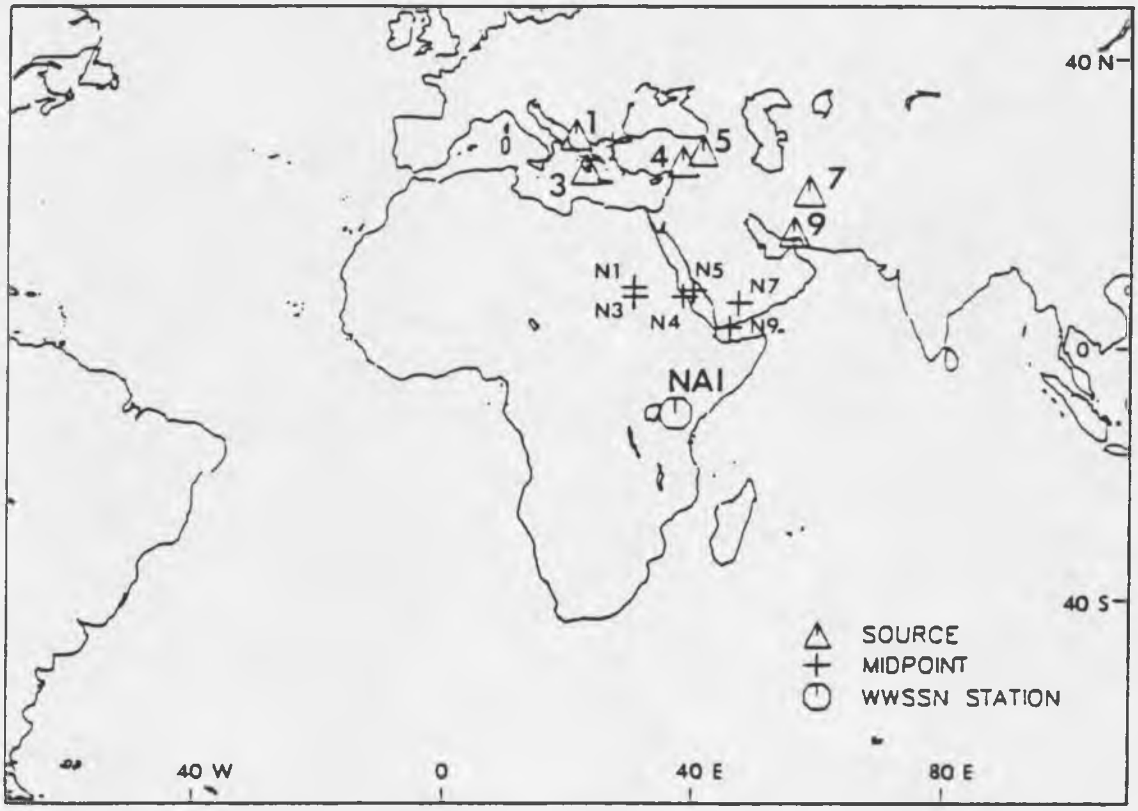


Figure C.1. SS data used to model the upper mantle shear velocity structure beneath northern Africa and the Arabian shield.

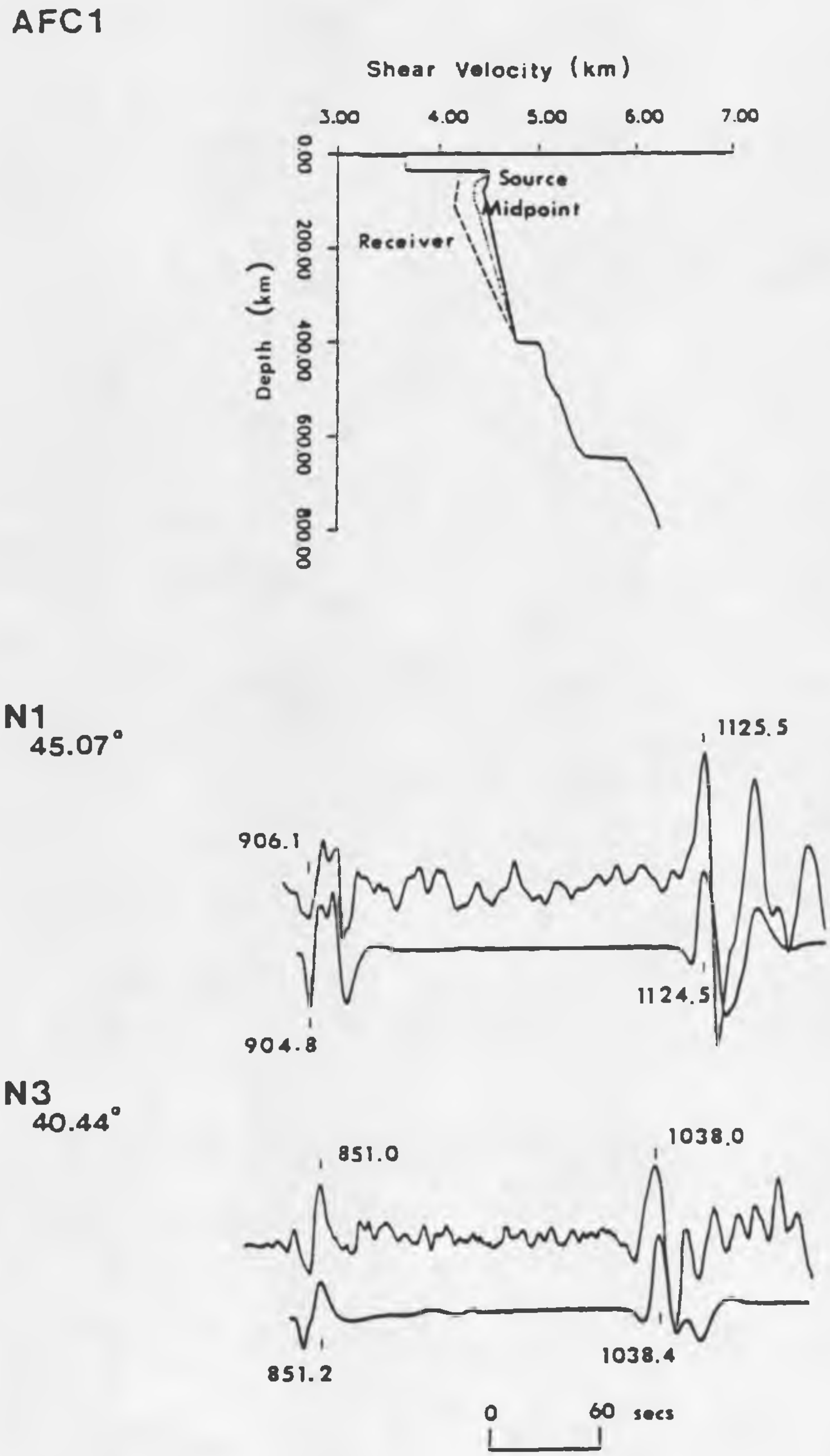


Figure C.2. A comparison of observed and synthetic seismograms for raypaths N1 and N3.

## Raypaths N4 and N5

The same source and receiver structures (AF4 and AF1) used for raypaths N1 and N3, are used in the modeling of raypaths N4 and N5, shown in Figure C.1. Slower midpoint velocities are required, however, as both midpoints are located within, or very near, the Red Sea rift.

Synthetics calculated with model AFC4 (Figure C.3) produce S and SS arrivals which are 1.4 seconds slow and 0.6 seconds fast, respectively, for raypath N4, and which are 1.7 and 1.5 seconds fast, for raypath N5. Variations introduced into the velocity structure which improve the traveltime fits for one raypath invariably worsen the traveltime fits for the second raypath. Model AFC4 is therefore considered to be representative of the shear velocity structure along raypaths N4 and N5.

In both cases, source depths were decreased by about 5 km. The origin time of earthquake 5 was uncertain, varying within 3.2 seconds (USCGS: 11 59 8.8, MOS: 11 59 11.0, BCIS: 11 59 12.0). This study incorporates the USCGS origin time. This however results in unreasonably slow source and/or receiver velocity structures. To compensate for this uncertainty, the depth was decreased from 12 to 5 km. In addition, an origin depth of 10 km for earthquake 4 was suspect. Synthetic seismograms computed using a depth of 10 km (for both raypaths B4 and N4) showed a consistently poor waveform match to the S arrival. This was eliminated when a depth of 5 km was substituted.

## Raypaths N7 and N9

The progressive decrease in seismic velocities towards the active rift zone, as discussed above, is also observed for raypaths N7 and N9 (Figure C.1). As with previous raypaths, seismic station NAI, is modeled with the slowest available velocity structure, AF1. This, however, requires relatively high velocities beneath the Arabian shield as is indicated in models AFC5 and AFC6 (Figure C.4). It is of interest that slower source

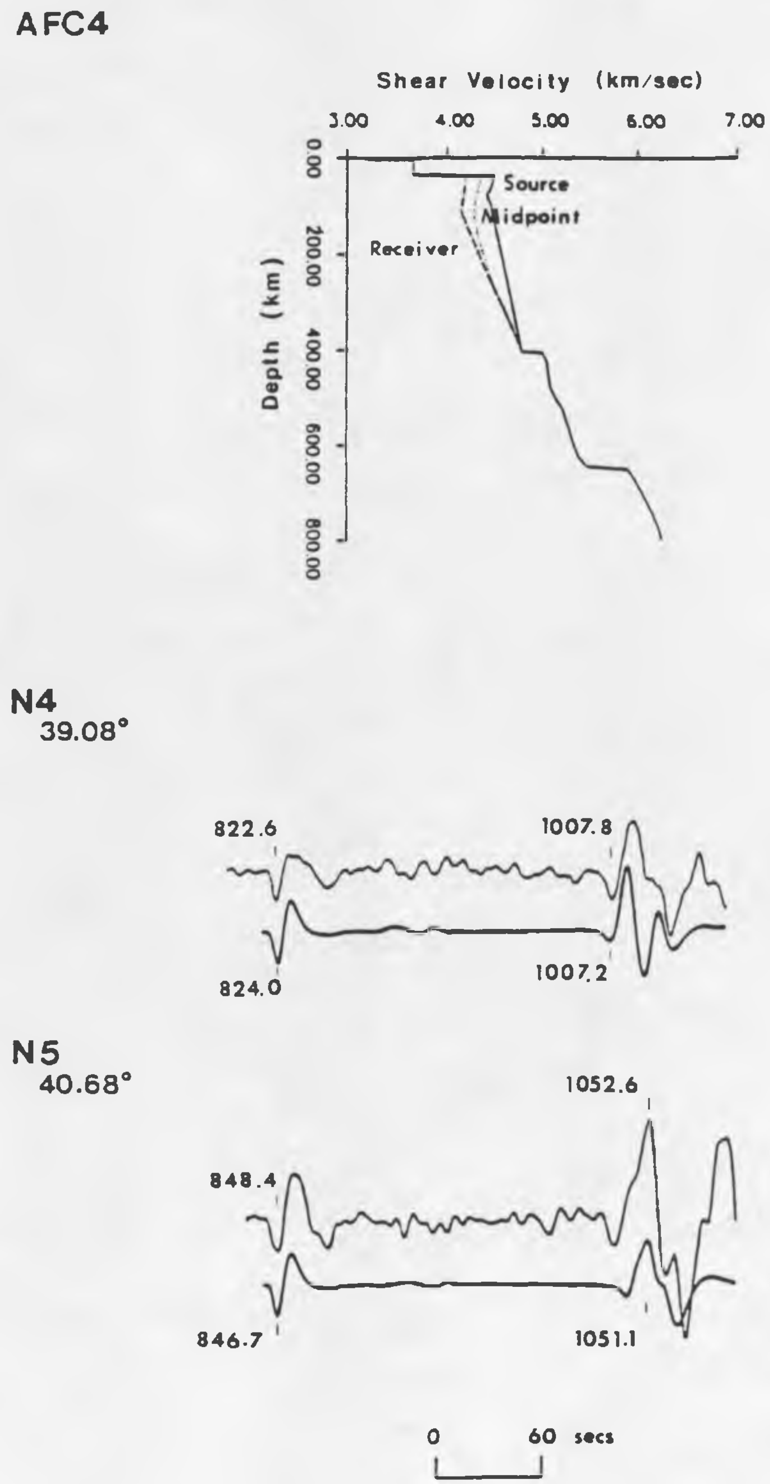


Figure C.3. A comparison of observed and synthetic seismograms for raypaths N4 and N5.

AFC5

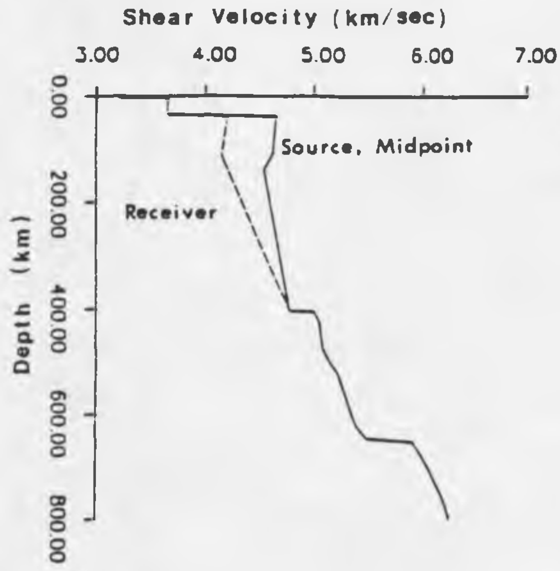


N7
40.49°

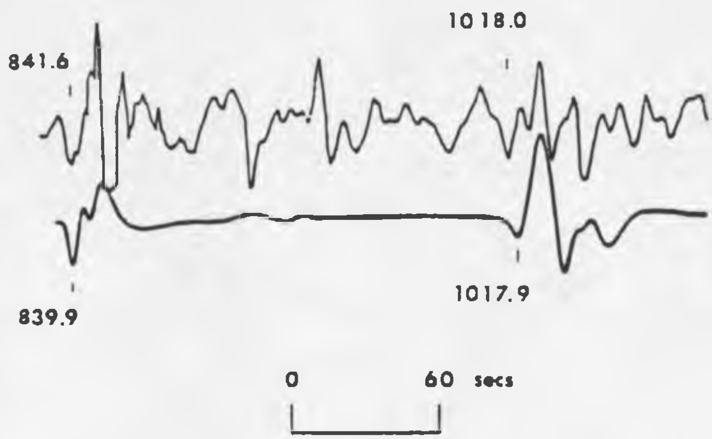


Figure C.4(a). A comparison of observed and synthetic seismograms for raypath N7.

AFC6

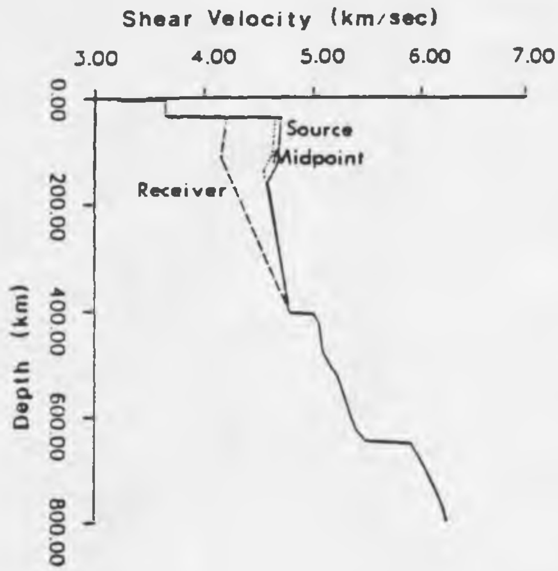


N9
34.49°

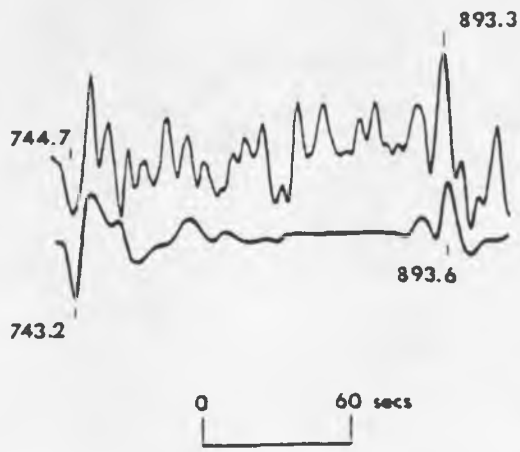


Figure C.4(b). A comparison of observed and synthetic seismograms for raypath N9.

velocities are determined for raypath N7 than for raypath N9. This apparently suggests a slower upper mantle velocity structure beneath Iran than beneath the Arabian peninsula. In both cases, the synthetic SS arrival times match the observed data to within 0.3 seconds yet the S phases arrive 1.5 to 1.7 seconds early. Substituting a slower source and/or receiver structure results in slightly improved S arrival times but a much worse match for the SS arrival. These changes, therefore, produce an increased error in the SS-S traveltime separation.

### Raypaths J6, E6, J9, J8, and H9

The upper mantle shear velocity structure beneath the Arabian shield is further constrained by the modeling of the set of S data shown in Figure C.5. The five raypaths J6, E6, J9, J8, and H9, extending westward from Iran to the eastern Mediterranean, provide strong evidence for a rather sharp transition from slower velocities in the north to a faster, somewhat more stable, structure in the south (towards the Arabian shield). The corresponding velocity profiles (from north to south): AF4, AF5, and AF7, are shown in Figure C.6. This sequence of velocity profiles shows a definite increase in upper mantle velocities and lid thickness towards the south. This provides further evidence that relatively high velocities can be expected beneath the Arabian shield. The complicated seismograms observed for the southern raypaths, J9, J8, and H9, are most likely due to the complicated structure within this transitional region.

### Raypaths A8 and A9

S waves propagating along raypaths A8 and A9 (Figure C.5) originate in Iran, travel beneath the Arabian peninsula, and are received at station AAE in Addis Abba, Ethiopia. Since a laterally homogeneous structure is assumed for the entire raypath, when modeling S waves, any velocity profile considered must be an average of the traveltime spent beneath both the Arabian peninsula and the active rift zone.

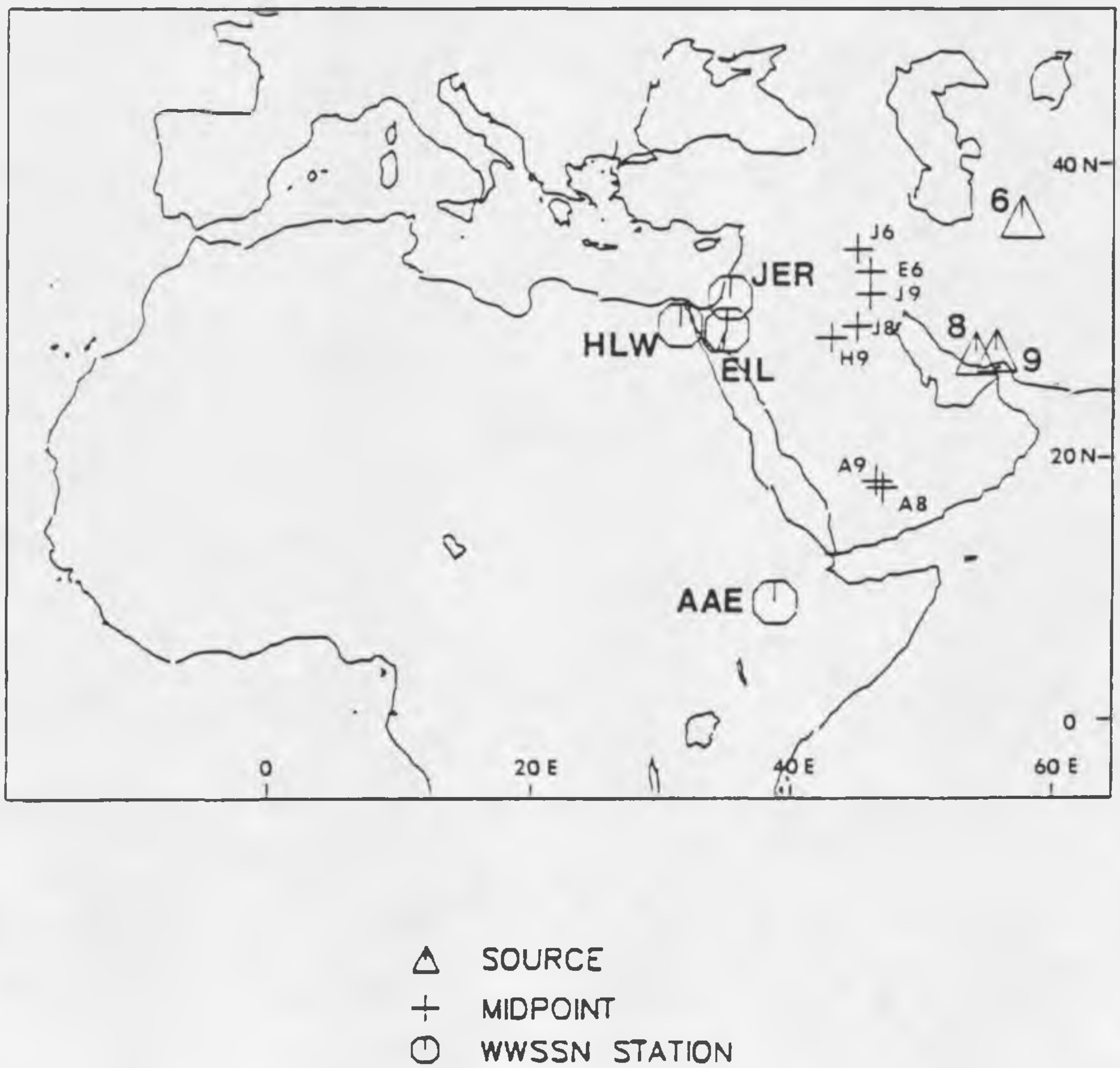


Figure C.5. S data used to model the upper mantle shear velocity structure beneath the Arabian shield and the surrounding region.

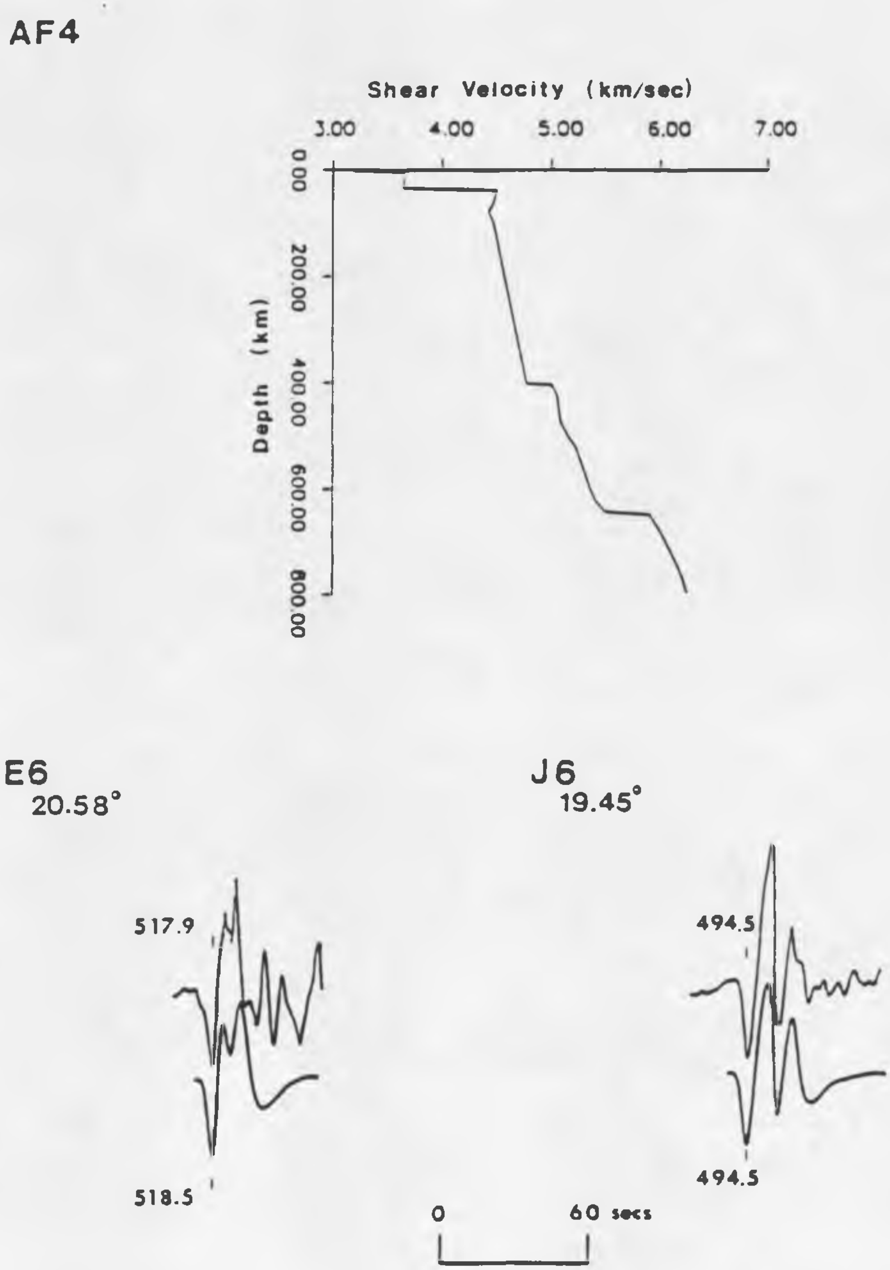


Figure C.6(a). A comparison of observed and synthetic seismograms for raypaths E6 and J6.

AF5

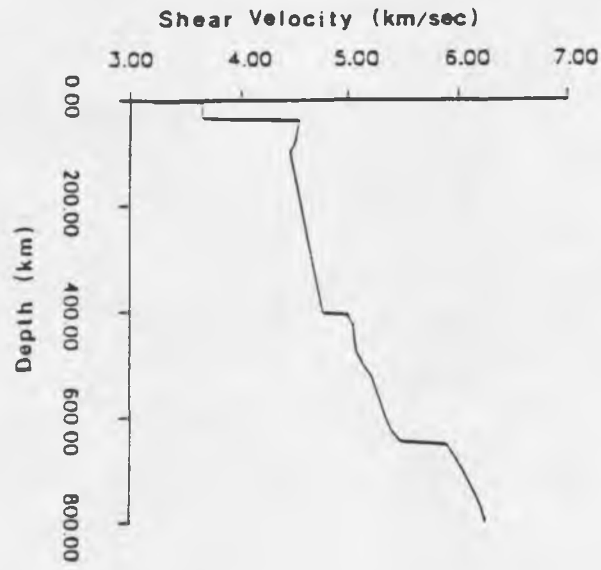


J9
18.31°


Figure C.6(b). A comparison of observed and synthetic seismograms for raypath J9.

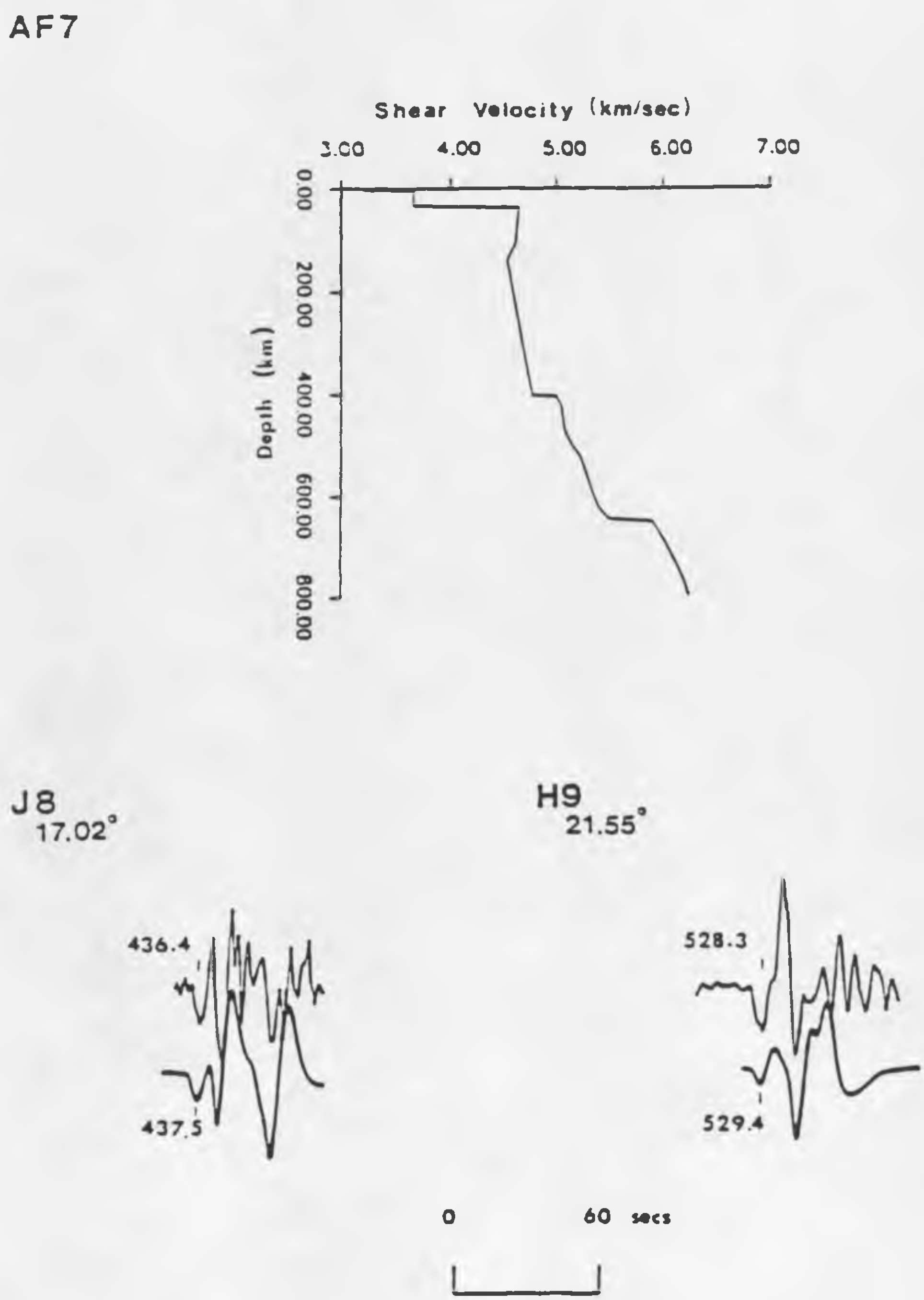


Figure C.6(c). A comparison of observed and synthetic seismograms for raypaths J8 and H9.

Approximately three-quarters of each raypath is located beneath the Arabian plate. The modeling of previous raypaths indicates a very slow velocity structure (AF1) beneath station NAI within Nairobi, Kenya. Gravity data suggest that the intensity of rift activity within Ethiopia should be as great, if not greater than, the rift activity within Kenya. Therefore, a velocity structure which is at least as slow as that determined for station NAI should be expected for station AAE. Further evidence for a relatively slow velocity structure beneath station AAE is provided in the discussion of the modeling of raypaths A11 and A12. It is proposed, then, that the velocity structure beneath Addis Abba is slightly slower, and that the velocity structure beneath the Arabian peninsula is somewhat faster, than that which is represented by model AF6. This again is indicative of high velocities beneath the shield region as well as a high velocity lid structure which extends to about 125 km depth. Model AF6 and the waveform fits for raypaths A8 and A9 are shown in Figure C.7.

### Raypaths B2 and B4

SS waves propagating along raypaths B2 and B4 (Figure C.8) travel nearly the entire length of eastern Africa before being received at station BUL within Bulawayo, Zimbabwe. These raypaths provide constraints on the transition from the East African Rift Zone to the adjacent West African and South African cratons.

Raypath B2, the westernmost raypath included in the northern data, does not parallel or cross any other raypath used within this study. Therefore, the velocity structure along this raypath is is not as well-constrained as it is for some of the other raypaths. Although several models provide adequate waveform fits within the travel-time constraints, all require relatively high velocities beneath both the source and receiver locations or unreasonably high velocities beneath one of these locations.

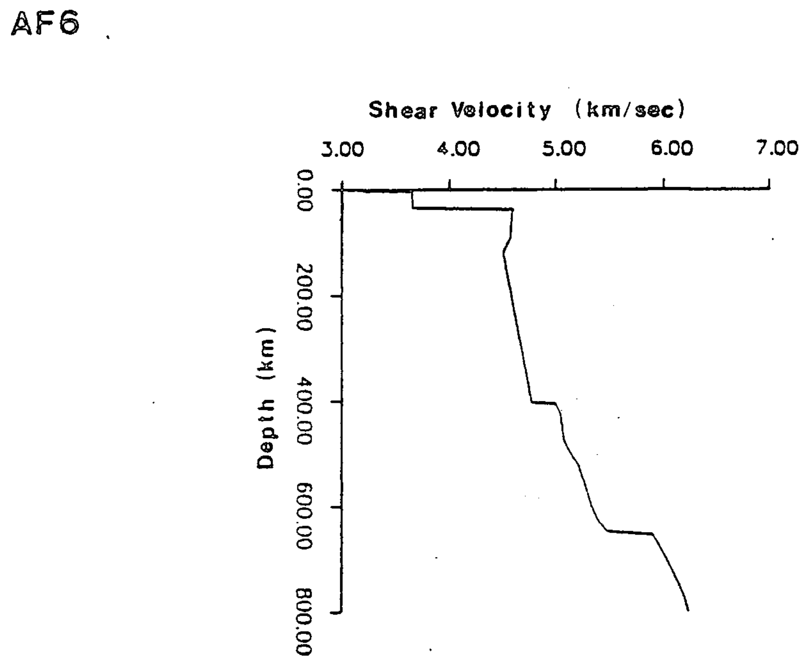


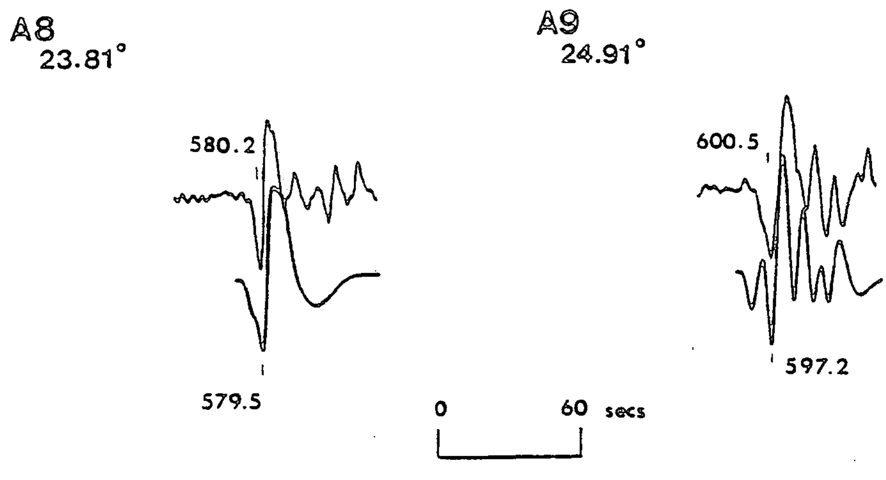


Figure C.7. A comparison of observed and synthetic seismograms for raypaths A8 and A9.

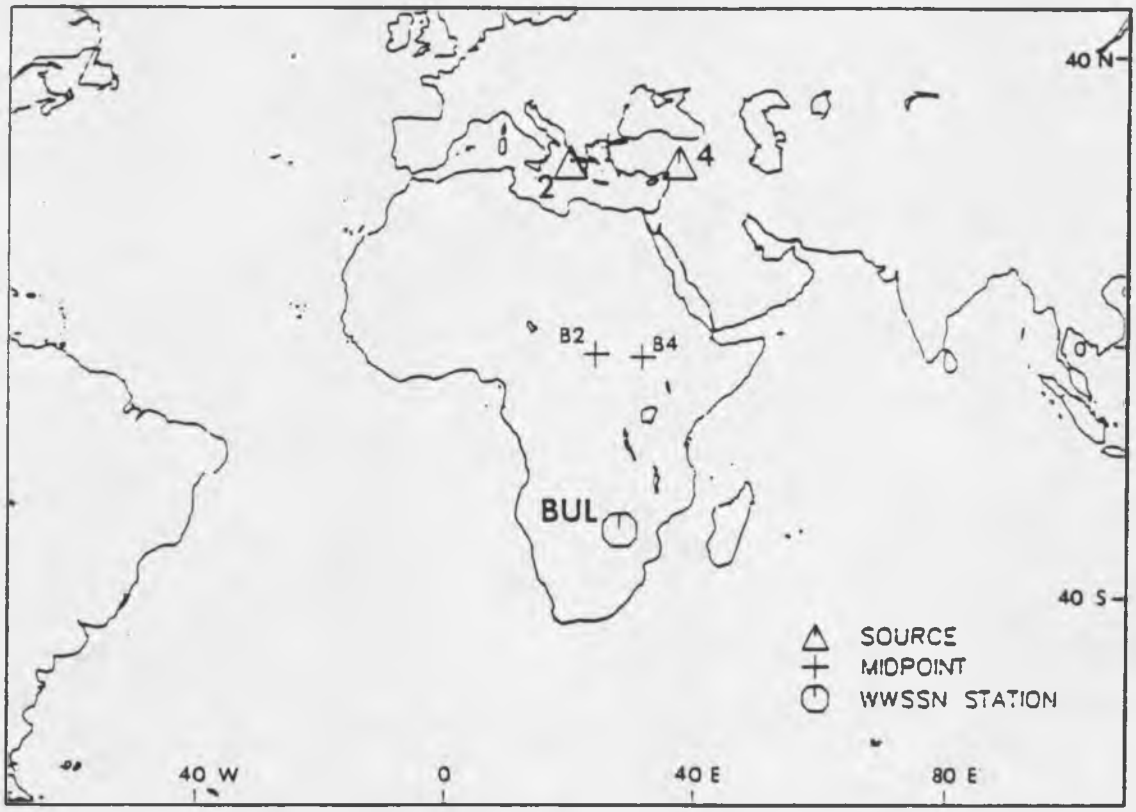


Figure C.8. SS data used to model the upper mantle transition from the East African Rift Zone to the surrounding stable craton.

Model AFC2, shown in Figure C.9, however, provides the best combination of SS-S separation and absolute S and SS traveltimes.

It is of interest that a high velocity source structure is required to fit the seismic data, yet the source is located in a region already designated (in this study) as relatively slow. This is readily explained by raypath B2 crossing the easternmost extent of the West African craton. Thus the source velocity structure, AF8, should be an average of the extremely high upper mantle velocities beneath the craton and the considerably slower velocities beneath the eastern Mediterranean.

The midpoint location, modeled with the relatively slow velocity structure AF4, is apparently affected by the East African Rift. The remainder of the path, from midpoint to station BUL, however, requires very high velocities. This indicates not only that the upper mantle velocities beneath southern Africa are very fast but also that the transition between the East African Rift Zone and the South African craton is relatively sharp.

Raypath B4 provides further information on lateral heterogeneity of the upper mantle velocities between the active rift zone and the South African craton. Reviewing model AFC3 (Figure C.9) it is evident that velocities decrease from source (AF4) to midpoint (AF2) as raypath B4 approaches the active rifting. Modeling the velocity structure from the midpoint location to station BUL, however, requires very high receiver velocities (AF9) even though this portion of the raypath lies adjacent to the southern extent of the East African Rift. This again suggests a relatively sharp upper mantle transition from the East African Rift to the South African craton.

## Raypaths G14, B13, and P11

Raypaths originating along the Southwest Indian Ocean Ridge system provide further constraints in the modeling of upper mantle velocities beneath southern Africa.

AFC2

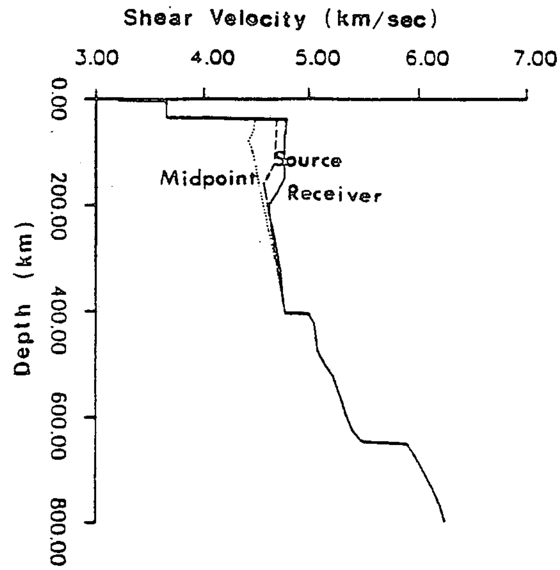


B2
58.39°

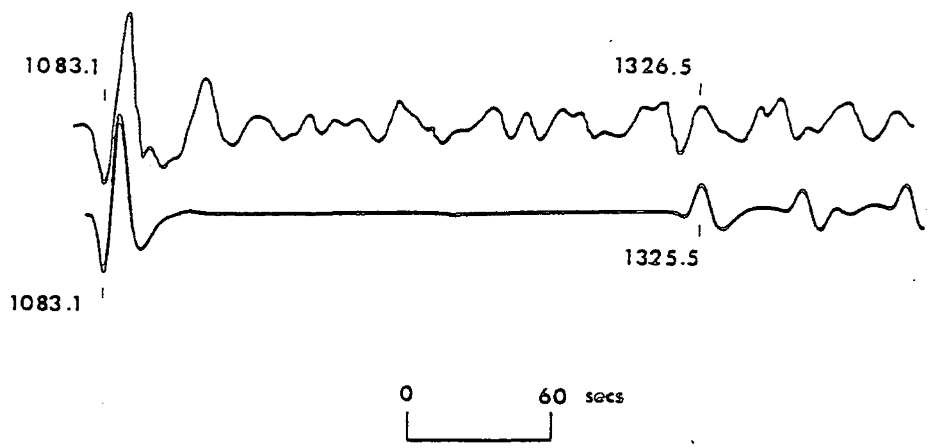


Figure C.9(a). A comparison of observed and synthetic seismograms for raypath B2.

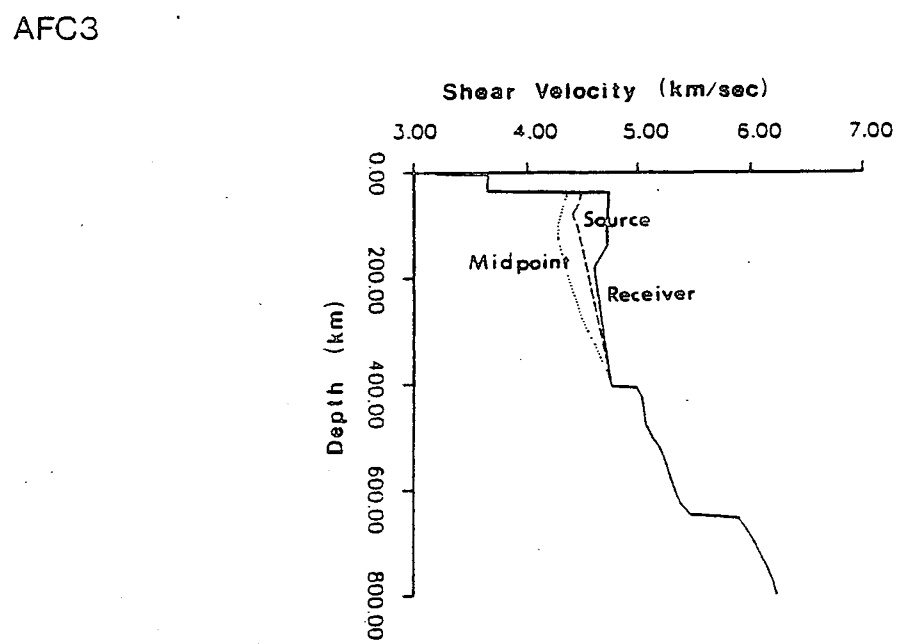


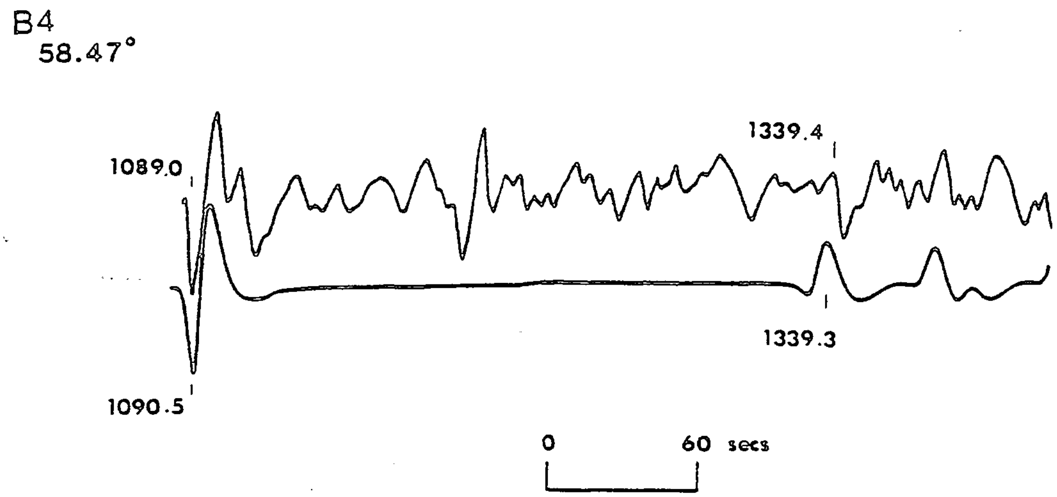


Figure C.9(b). A comparison of observed and synthetic seismograms for raypath B4.

As significant portions of these raypaths lie beneath oceanic material, it is first important to understand the upper mantle velocity structure of the Southwest Indian Ocean.

Seismic waves propagating along raypaths P11, B13, and G14 spend approximately three-quarters of their traveltime beneath oceanic material (Figure C.10). Raypath G14 follows an approximate east-west path beneath the Southwest Indian Ocean before being recorded at station GRM (Grahamstown, South Africa). Although the peculiar waveform observed for raypath G14 has not been duplicated by any reasonable oceanic model (including several models tested but not included in this paper) the traveltime corresponding to the first trough is matched within 0.3 seconds with velocity profile AF12 (Figure C.11). This velocity profile exhibits a high velocity lid structure to a depth of 150 km.

Raypath B13 originates in approximately the same area but travels northwestward towards station BUL. The best waveform and traveltime fits are again provided by oceanic model AF12 (Figure C.11). This model produces a synthetic seismogram in which the first trough occurs 1.5 seconds early and the second trough occurs 0.7 seconds late. When modeling raypath B13 with the slower oceanic structure, AF11, these same troughs occur 0.9 seconds and 3.5 seconds late.

The velocity structure for this portion of the Southwest Indian Ocean appears to be well-represented by model AF12. The slow half-spreading rate of 1.0 cm/yr (Bergh, 1971) along the ridge has resulted in very old oceanic material ($\geq$ 100 million years old). Thus, relatively high upper mantle velocities can be expected.

The third raypath, P11, has been modeled with velocity structure AF11 (Figure C.12). The first trough on the corresponding synthetic seismogram occurs 1.7 seconds late while the first peak occurs 1.1 seconds early. Modeling raypath P11 with velocity structure AF12, however, produces a trough and peak which are 2.6 and 8.0 seconds

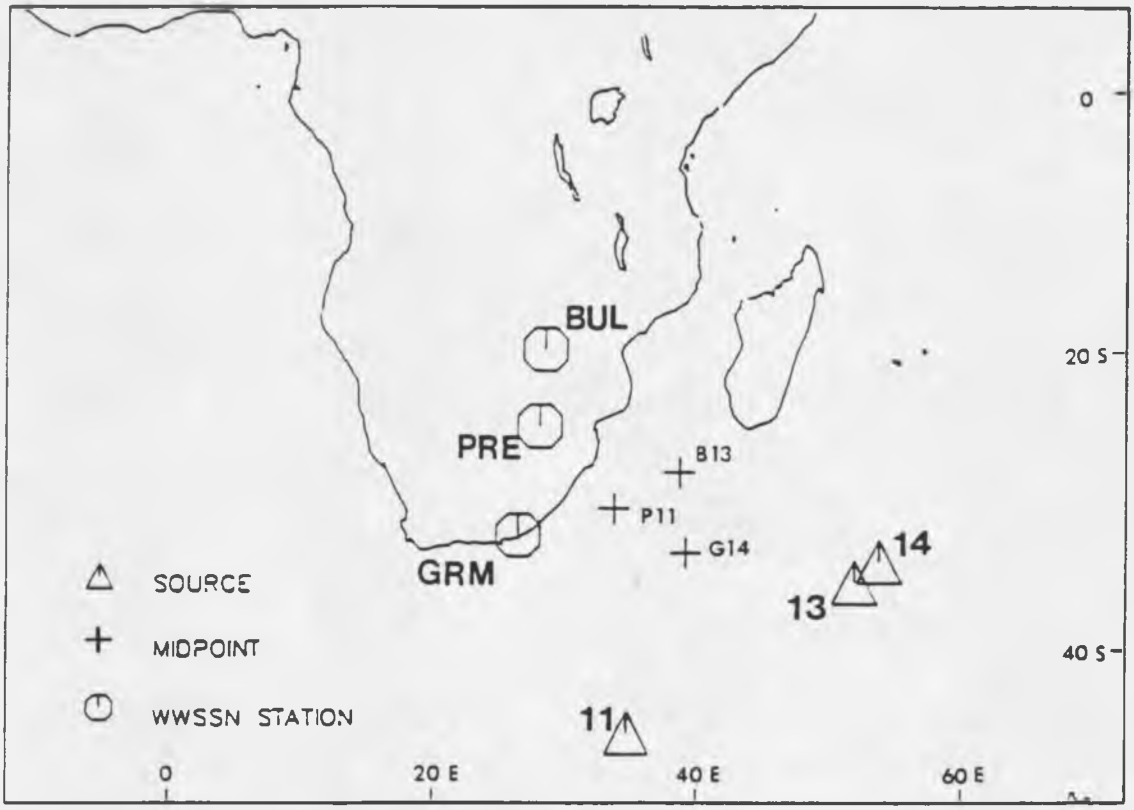


Figure C.10. S data used to model the upper mantle shear velocity structure beneath the Southwest Indian Ocean.

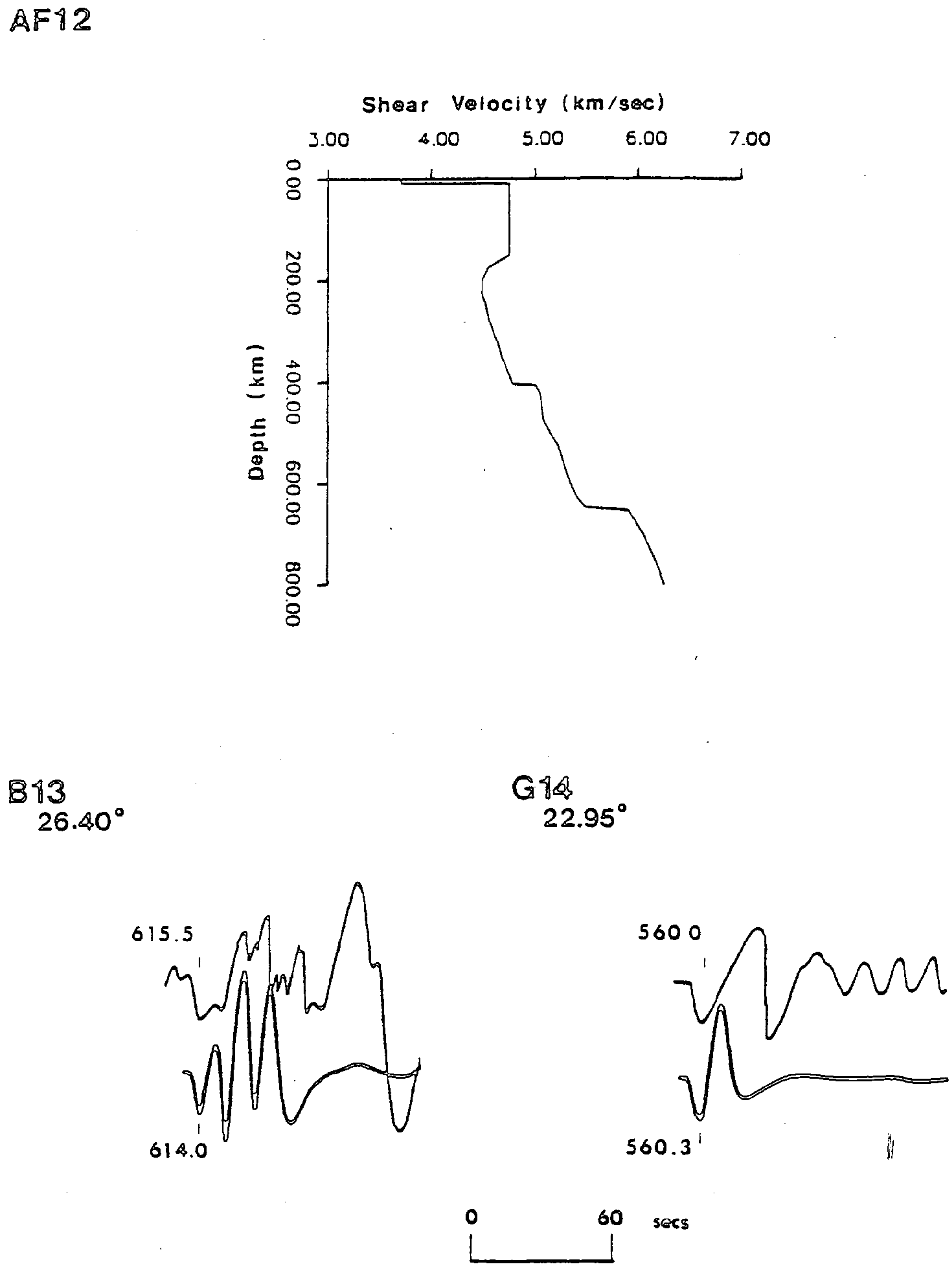


Figure C.11. A comparison of observed and synthetic seismograms for raypaths B13 and G14.

AF11

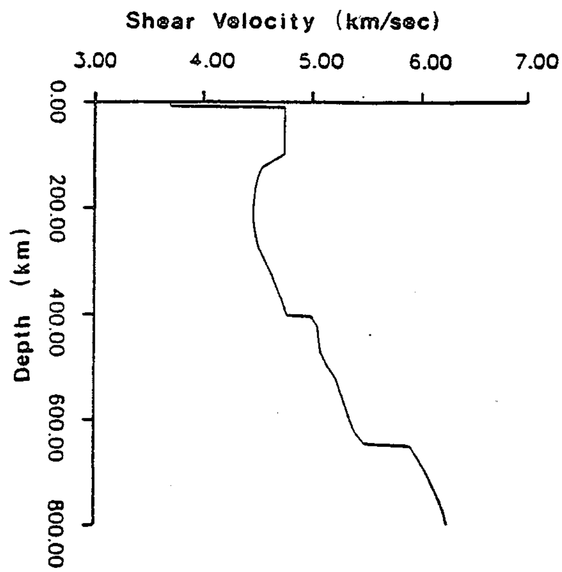


P11
20.39°

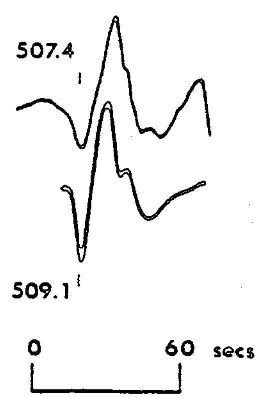


Figure C.12. A comparison of observed and synthetic seismograms for raypath P11.

early, respectively. The depth of earthquake 11 has been increased from 10 km to 15 km. This was necessary as an adequate waveform fit could not be obtained, with any reasonable oceanic velocity structure, when a source shallower than 15 km depth was used. Although this has produced favorable changes for raypaths P11 and S11, changes for raypath A11 are less favorable.

Model AF11 appears to be a more accurate representation of the velocity structure, than is AF12, for this region of the Southwest Indian Ocean. The slower velocities have been attributed to the possible occurrence of a 'leaky transform' within the region. This is consistent with the large component of dip-slip motion determined along several transform faults within the area (see Wald and Wallace, 1986).

## Raypaths S11, A11, A12, and B10

The SS data set for southern Africa includes raypaths S11, All, and A12, which originate in the region of the proposed 'leaky transform', and raypath B10 which originates to the southwest. These raypaths are shown in Figure C.13.

Raypaths S11, A11 and A12, are each modeled with the source velocity structure AF11, as expected. Raypath S11 continues northwestward towards station SDB in Sa Da Bandeira, Angola. The surface reflection associated with this raypath occurs just north of the south African coast. This midpoint location is modeled with velocity structure AF10, an average of the relatively fast upper mantle beneath both southern Africa and the adjacent Southwest Indian Ocean. The continental portion of this raypath, from midpoint to receiver, is also modeled with the high velocities of AF10. This sequence of velocity profiles, shown in model AFC9 (Figure C.14) produces an S arrival approximately 0.8 seconds early and an SS arrival, though more difficult to distinguish, approximately 1.8 seconds early.

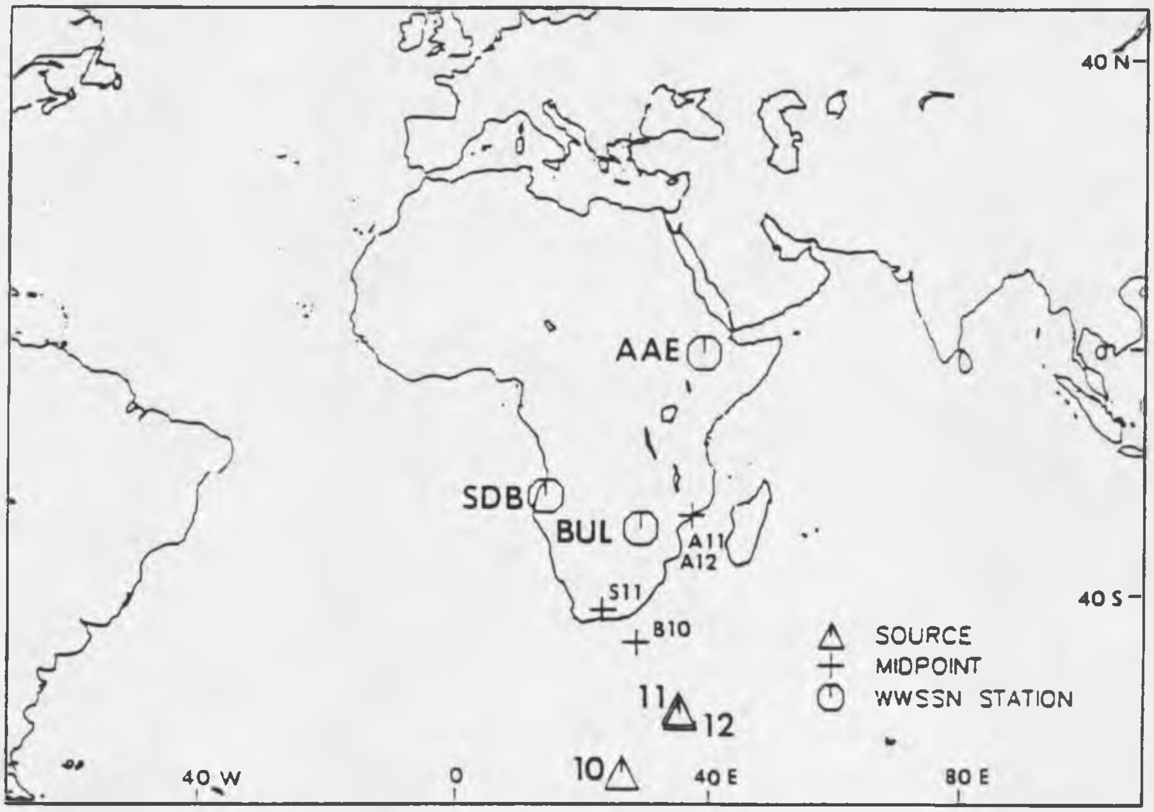


Figure C.13. SS data used to model the upper mantle shear velocity structure beneath the Southwest Indian Ocean and southern Africa.

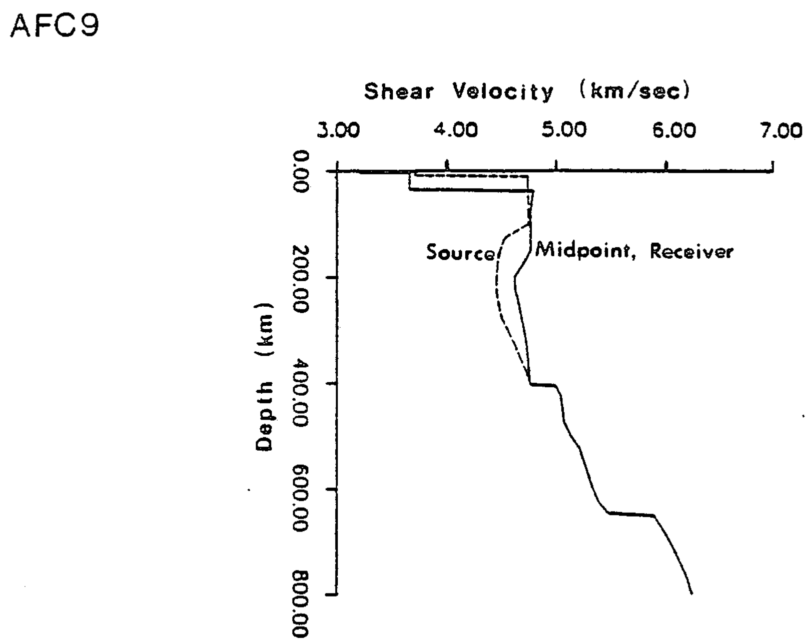


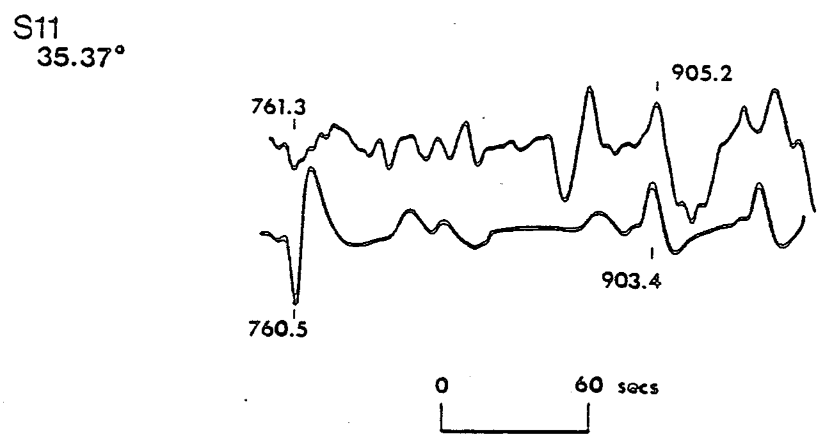


Figure C.14. A comparison of observed and synthetic seismograms for raypath S11.

Raypaths A11 and A12, though originating in the same area as raypath S11, follow a very different course. These rays, traveling northward, are reflected at the surface along the coast of Mozambique before continuing onto station AAE in Ethiopia. This midpoint location is not only a transition between oceanic and continental material but also occurs just south of the southernmost extent of the East African Rift Zone. A midpoint structure corresponding to velocity profile AF11 provides the best waveform and traveltime results. It is proposed that AF11 is an acceptable average of the stable cràton, the active rift zone, and the relatively fast oceanic material. The remainder of the path is located beneath the rift zone, including the more active segments found in Kenya and Ethiopia. Therefore, it is not surprising that receiver station AAE is modeled with the slowest velocity structure, AF1. Model AFC8 combines this series of source, midpoint, and receiver velocity structures and is shown in Figure C.15 along with the corresponding waveform fits. The synthetic seismogram for raypath A11 shows an S arrival which is approximately 1.2 seconds early and an SS arrival which occurs approximately 0.6 seconds early. The opposite relation is shown for raypath A12. The synthetic seismogram for this raypath includes S and SS phases which arrive 1.7 and 0.9 seconds late, respectively. Efforts to increase the accuracy of absolute traveltimes for one raypath result in decreased accuracy for the second raypath. Model AFC8, therefore, provides the best overall results for this series of raypaths.

The final raypath B10 extends northward from the Southwest Indian Ocean Ridge to station BUL in Zimbabwe. The source region, which occurs to the southwest of previously studied earthquake sources, is modeled with the high velocity oceanic structure AF12. This indicates that the slower velocities associated with the possible 'leaky transform' are isolated and do not extend this far to the southwest. The midpoint, located just south of the continent, is modeled with the fast upper mantle velocities of structure AF10. This indicates not only fast upper mantle beneath the southern tip of

AFC8

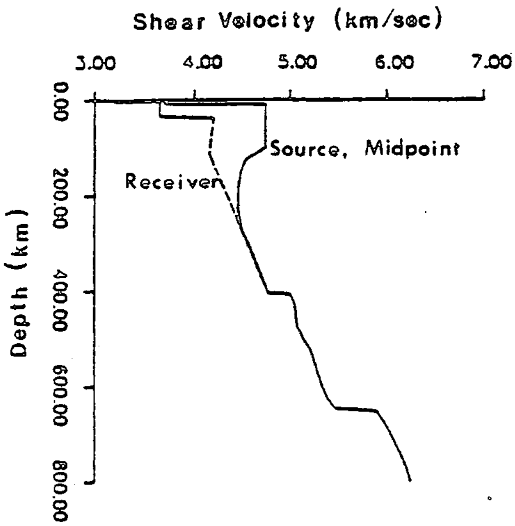


A11
54.32°

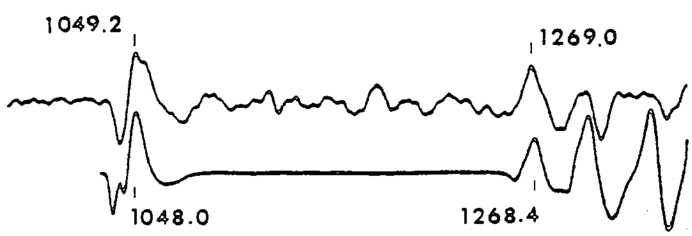


A12
54.80°

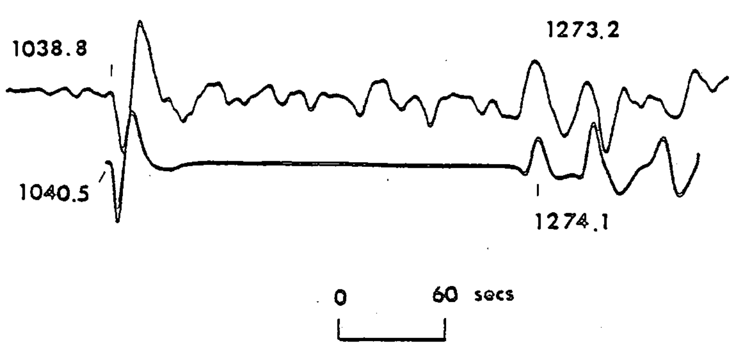


Figure C.15. A comparison of observed and synthetic seismograms for raypaths A11 and A12.

the continent (possibly faster than what is represented by AF10) but also beneath the adjacent Southwest Indian Ocean. As with raypath S11, the continental portion of this raypath (beneath southern Africa) requires very high velocities. This has resulted in receiver station, BUL, also being modeled with velocity structure AF10. This series of velocity profiles is shown in model AFC7. The synthetic seismogram shown in Figure C.16 produces S and SS phases arriving 0.8 and 1.5 seconds late, respectively.

Table C.1 lists the mismatch in traveltime, between the synthetic and observed data, for each of the 22 raypaths. Indicated by an asterisk is the one match which did not fall within the preferred traveltime constraint of 2.0 seconds (the S phase associated with raypath A6).

AFC7

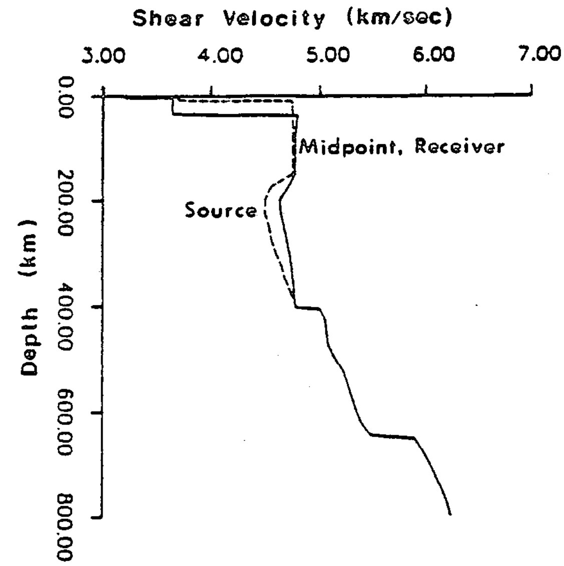


B10
32.35°

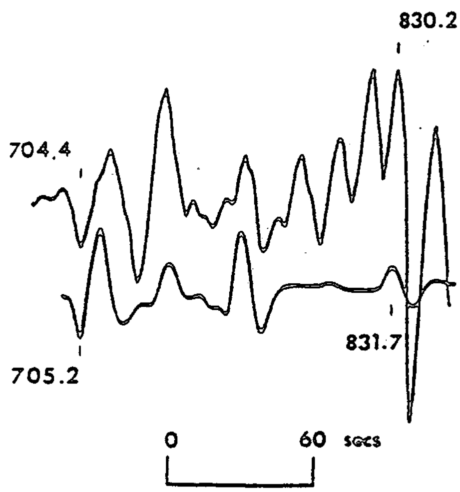


Figure C.16. A comparison of observed and synthetic seismograms for raypath B10.

TABLE C.1

TRAVELTIME ERRORS

| Raypath | Synthetic S | Synthetic SS | Synthetic SS-S |
|---|---|---|---|
| E6 | 0.6 sec slow | | |
| J6 | 0.0 | | |
| A8 | 0.7 sec fast | | |
| J8 | 1.1 sec slow | | |
| A9* | 3.3 sec fast | | |
| H9 | 1.1 sec slow | | |
| J9 | 0.6 sec slow | | |
| P11 | 1.7 sec slow | | |
| B13 | 1.5 sec fast | | |
| G14 | 0.3 sec slow | | |
| N1 | 1.3 sec fast | 1.0 sec fast | 0.3 sec |
| B2 | 0.0 | 1.0 sec fast | 1.0 sec |
| N3 | 0.2 sec slow | 0.4 sec slow | 0.2 sec |
| B4 | 1.5 sec slow | 0.1 sec fast | 1.6 sec |
| N4 | 1.4 sec slow | 0.6 sec fast | 2.0 sec |
| N5 | 1.7 sec fast | 1.5 sec fast | 0.2 sec |
| N7 | 1.7 sec fast | 0.1 sec fast | 1.6 sec |
| N9 | 1.5 sec fast | 0.3 sec slow | 1.8 sec |
| B10 | 0.8 sec slow | 1.5 sec slow | 0.7 sec |
| A11 | 1.2 sec fast | 0.6 sec fast | 0.6 sec |
| S11 | 0.8 sec fast | 1.8 sec fast | 1.0 sec |
| A12 | 1.7 sec slow | 0.9 sec slow | 0.8 sec |

*Synthetic traveltime does not fall within 2.0 seconds of the observed traveltime.

APPENDIX D

VELOCITY MODELS

TABLE D.1

MODEL AF1

| Depth (km) | Shear Velocity (km/sec) |
|---|---|
| 0.0 | 3.200 |
| 3.5 | 3.200 |
| 4.0 | 3.650 |
| 35.0 | 3.650 |
| 38.0 | 4.200 |
| 63.0 | 4.182 |
| 88.0 | 4.165 |
| 112.0 | 4.147 |
| 125.0 | 4.175 |
| 150.0 | 4.229 |
| 175.0 | 4.284 |
| 200.0 | 4.338 |
| 225.0 | 4.392 |
| 250.0 | 4.446 |
| 275.0 | 4.500 |
| 300.0 | 4.555 |
| 325.0 | 4.609 |
| 350.0 | 4.663 |
| 375.0 | 4.717 |
| 404.0 | 4.780 |
| 406.0 | 5.000 |
| 425.0 | 5.050 |
| 450.0 | 5.065 |
| 475.0 | 5.080 |
| 500.0 | 5.140 |
| 525.0 | 5.220 |
| 550.0 | 5.550 |
| 575.0 | 5.300 |
| 600.0 | 5.340 |
| 625.0 | 5.395 |
| 647.0 | 5.480 |
| 653.0 | 5.900 |
| 675.0 | 5.970 |
| 700.0 | 6.040 |
| 725.0 | 6.100 |
| 750.0 | 6.160 |
| 775.0 | 6.210 |
| 800.0 | 6.244 |
| 825.0 | 6.261 |
| 850.0 | 6.279 |
| 875.0 | 6.296 |
| 900.0 | 6.313 |

TABLE D.2

MODEL AF2

| Depth (km) | Shear Velocity (km/sec) |
|---|---|
| 0.0 | 3.200 |
| 3.5 | 3.200 |
| 4.0 | 3.650 |
| 35.0 | 3.650 |
| 38.0 | 4.400 |
| 50.0 | 4.350 |
| 75.0 | 4.320 |
| 100.0 | 4.290 |
| 125.0 | 4.290 |
| 150.0 | 4.320 |
| 175.0 | 4.350 |
| 200.0 | 4.390 |
| 225.0 | 4.430 |
| 250.0 | 4.470 |
| 275.0 | 4.510 |
| 300.0 | 4.570 |
| 325.0 | 4.630 |
| 350.0 | 4.680 |
| 375.0 | 4.730 |
| 404.0 | 4.780 |
| 406.0 | 5.000 |
| 425.0 | 5.050 |
| 450.0 | 5.065 |
| 475.0 | 5.080 |
| 500.0 | 5.140 |
| 525.0 | 5.220 |
| 550.0 | 5.260 |
| 575.0 | 5.300 |
| 600.0 | 5.340 |
| 625.0 | 5.390 |
| 647.0 | 5.480 |
| 653.0 | 5.900 |
| 675.0 | 5.970 |
| 700.0 | 6.040 |
| 725.0 | 6.100 |
| 750.0 | 6.160 |
| 775.0 | 6.210 |
| 800.0 | 6.244 |
| 825.0 | 6.261 |
| 850.0 | 6.279 |
| 875.0 | 6.296 |
| 900.0 | 6.313 |

TABLE D.3

MODEL AF3

| Depth (km) | Shear Velocity (km/sec) |
|---|---|
| 0.0 | 3.200 |
| 3.5 | 3.200 |
| 4.0 | 3.650 |
| 35.0 | 3.650 |
| 38.0 | 4.450 |
| 50.0 | 4.450 |
| 59.0 | 4.367 |
| 68.0 | 4.350 |
| 84.0 | 4.342 |
| 100.0 | 4.350 |
| 125.0 | 4.396 |
| 175.0 | 4.465 |
| 225.0 | 4.534 |
| 250.0 | 4.568 |
| 275.0 | 4.603 |
| 300.0 | 4.637 |
| 325.0 | 4.671 |
| 350.0 | 4.706 |
| 375.0 | 4.740 |
| 404.0 | 4.780 |
| 406.0 | 5.000 |
| 425.0 | 5.050 |
| 450.0 | 5.065 |
| 475.0 | 5.080 |
| 500.0 | 5.140 |
| 525.0 | 5.220 |
| 550.0 | 5.260 |
| 575.0 | 5.300 |
| 600.0 | 5.340 |
| 625.0 | 5.390 |
| 647.0 | 5.480 |
| 653.0 | 5.900 |
| 675.0 | 5.970 |
| 700.0 | 6.040 |
| 725.0 | 6.100 |
| 750.0 | 6.160 |
| 775.0 | 6.210 |
| 800.0 | 6.244 |
| 825.0 | 6.261 |
| 850.0 | 6.279 |
| 875.0 | 6.296 |
| 900.0 | 6.313 |

TABLE D.4

MODEL AF4

| Depth (km) | Shear Velocity (km/sec) |
|---|---|
| 0.0 | 3.200 |
| 3.5 | 3.200 |
| 4.0 | 3.650 |
| 35.0 | 3.650 |
| 38.0 | 4.500 |
| 56.0 | 4.477 |
| 67.0 | 4.455 |
| 78.0 | 4.420 |
| 100.0 | 4.468 |
| 125.0 | 4.494 |
| 150.0 | 4.520 |
| 175.0 | 4.546 |
| 200.0 | 4.572 |
| 225.0 | 4.598 |
| 250.0 | 4.624 |
| 275.0 | 4.650 |
| 300.0 | 4.676 |
| 325.0 | 4.702 |
| 350.0 | 4.728 |
| 375.0 | 4.754 |
| 404.0 | 4.780 |
| 406.0 | 5.000 |
| 425.0 | 5.050 |
| 450.0 | 5.065 |
| 475.0 | 5.080 |
| 500.0 | 5.140 |
| 525.0 | 5.220 |
| 550.0 | 5.260 |
| 575.0 | 5.300 |
| 600.0 | 5.340 |
| 625.0 | 5.390 |
| 647.0 | 5.480 |
| 653.0 | 5.900 |
| 675.0 | 5.970 |
| 700.0 | 6.040 |
| 725.0 | 6.100 |
| 750.0 | 6.160 |
| 775.0 | 6.210 |
| 800.0 | 6.244 |
| 825.0 | 6.261 |
| 850.0 | 6.279 |
| 875.0 | 6.296 |

TABLE D.5

MODEL AF5

| Depth (km) | Shear Velocity (km/sec) |
|---|---|
| 0.0 | 3.200 |
| 3.5 | 3.200 |
| 4.0 | 3.650 |
| 35.0 | 3.650 |
| 38.0 | 4.550 |
| 80.0 | 4.515 |
| 98.0 | 4.463 |
| 100.0 | 4.465 |
| 125.0 | 4.491 |
| 150.0 | 4.517 |
| 175.0 | 4.543 |
| 200.0 | 4.569 |
| 225.0 | 4.595 |
| 250.0 | 4.620 |
| 275.0 | 4.646 |
| 300.0 | 4.672 |
| 325.0 | 4.698 |
| 350.0 | 4.724 |
| 375.0 | 4.750 |
| 404.0 | 4.780 |
| 406.0 | 5.000 |
| 425.0 | 5.050 |
| 450.0 | 5.065 |
| 475.0 | 5.080 |
| 500.0 | 5.140 |
| 525.0 | 5.220 |
| 550.0 | 5.260 |
| 575.0 | 5.300 |
| 600.0 | 5.340 |
| 625.0 | 5.390 |
| 647.0 | 5.480 |
| 653.0 | 5.900 |
| 675.0 | 5.970 |
| 700.0 | 6.040 |
| 725.0 | 6.100 |
| 750.0 | 6.160 |
| 775.0 | 6.210 |
| 800.0 | 6.244 |
| 825.0 | 6.261 |
| 850.0 | 6.279 |
| 875.0 | 6.296 |
| 900.0 | 6.313 |

TABLE D.6

MODEL AF6

| Depth (km) | Shear Velocity (km/sec) |
|---|---|
| 0.0 | 3.200 |
| 3.5 | 3.200 |
| 4.0 | 3.650 |
| 35.0 | 3.650 |
| 38.0 | 4.600 |
| 94.0 | 4.576 |
| 106.0 | 4.545 |
| 113.0 | 4.528 |
| 119.0 | 4.511 |
| 125.0 | 4.515 |
| 150.0 | 4.539 |
| 175.0 | 4.563 |
| 200.0 | 4.587 |
| 225.0 | 4.611 |
| 250.0 | 4.635 |
| 275.0 | 4.660 |
| 300.0 | 4.684 |
| 325.0 | 4.708 |
| 350.0 | 4.732 |
| 375.0 | 4.756 |
| 404.0 | 4.780 |
| 406.0 | 5.000 |
| 425.0 | 5.050 |
| 450.0 | 5.065 |
| 475.0 | 5.080 |
| 500.0 | 5.140 |
| 525.0 | 5.220 |
| 550.0 | 5.260 |
| 575.0 | 5.300 |
| 600.0 | 5.340 |
| 625.0 | 5.390 |
| 647.0 | 5.480 |
| 653.0 | 5.900 |
| 675.0 | 5.970 |
| 700.0 | 6.040 |
| 725.0 | 6.100 |
| 750.0 | 6.160 |
| 775.0 | 6.210 |
| 800.0 | 6.244 |
| 825.0 | 6.261 |
| 850.0 | 6.279 |
| 875.0 | 6.296 |

TABLE D.7

MODEL AF7

| Depth (km) | Shear Velocity (km/sec) |
|---|---|
| 0.0 | 3.200 |
| 3.5 | 3.200 |
| 4.0 | 3.650 |
| 35.0 | 3.650 |
| 38.0 | 4.650 |
| 73.0 | 4.635 |
| 108.0 | 4.620 |
| 139.0 | 4.539 |
| 140.0 | 4.540 |
| 150.0 | 4.549 |
| 175.0 | 4.572 |
| 200.0 | 4.594 |
| 225.0 | 4.617 |
| 250.0 | 4.640 |
| 275.0 | 4.663 |
| 300.0 | 4.685 |
| 325.0 | 4.708 |
| 350.0 | 4.731 |
| 375.0 | 4.754 |
| 400.0 | 4.777 |
| 404.0 | 4.780 |
| 406.0 | 5.000 |
| 425.0 | 5.050 |
| 450.0 | 5.065 |
| 475.0 | 5.080 |
| 500.0 | 5.140 |
| 525.0 | 5.220 |
| 550.0 | 5.260 |
| 575.0 | 5.300 |
| 600.0 | 5.340 |
| 625.0 | 5.390 |
| 647.0 | 5.480 |
| 653.0 | 5.900 |
| 675.0 | 5.970 |
| 700.0 | 6.040 |
| 725.0 | 6.100 |
| 750.0 | 6.160 |
| 775.0 | 6.210 |
| 800.0 | 6.244 |
| 825.0 | 6.261 |
| 850.0 | 6.279 |
| 875.0 | 6.296 |

TABLE D.8

MODEL AF8

| Depth (km) | Shear Velocity (km/sec) |
|---|---|
| 0.0 | 3.200 |
| 3.5 | 3.200 |
| 4.0 | 3.650 |
| 35.0 | 3.650 |
| 38.0 | 4.700 |
| 80.0 | 4.688 |
| 122.0 | 4.676 |
| 140.0 | 4.629 |
| 160.0 | 4.577 |
| 175.0 | 4.593 |
| 200.0 | 4.614 |
| 212.0 | 4.624 |
| 225.0 | 4.635 |
| 237.0 | 4.645 |
| 250.0 | 4.655 |
| 275.0 | 4.676 |
| 300.0 | 4.697 |
| 325.0 | 4.718 |
| 350.0 | 4.738 |
| 375.0 | 4.759 |
| 404.0 | 4.780 |
| 406.0 | 5.000 |
| 425.0 | 5.050 |
| 450.0 | 5.065 |
| 475.0 | 5.080 |
| 500.0 | 5.140 |
| 525.0 | 5.220 |
| 550.0 | 5.260 |
| 575.0 | 5.300 |
| 600.0 | 5.340 |
| 625.0 | 5.390 |
| 647.0 | 5.480 |
| 653.0 | 5.900 |
| 675.0 | 5.970 |
| 700.0 | 6.040 |
| 725.0 | 6.100 |
| 750.0 | 6.160 |
| 775.0 | 6.210 |
| 800.0 | 6.244 |
| 825.0 | 6.261 |
| 850.0 | 6.279 |
| 875.0 | 6.296 |

TABLE D.9

MODEL AF9

| Depth (km) | Shear Velocity (km/sec) |
|---|---|
| 0.0 | 3.200 |
| 3.5 | 3.200 |
| 4.0 | 3.650 |
| 35.0 | 3.650 |
| 38.0 | 4.750 |
| 87.0 | 4.745 |
| 136.0 | 4.739 |
| 158.0 | 4.680 |
| 180.0 | 4.621 |
| 190.0 | 4.628 |
| 200.0 | 4.635 |
| 225.0 | 4.653 |
| 250.0 | 4.671 |
| 275.0 | 4.688 |
| 300.0 | 4.706 |
| 325.0 | 4.724 |
| 350.0 | 4.742 |
| 375.0 | 4.759 |
| 404.0 | 4.780 |
| 406.0 | 5.000 |
| 425.0 | 5.050 |
| 450.0 | 5.065 |
| 475.0 | 5.080 |
| 500.0 | 5.140 |
| 525.0 | 5.220 |
| 550.0 | 5.260 |
| 575.0 | 5.300 |
| 600.0 | 5.340 |
| 625.0 | 5.390 |
| 647.0 | 5.480 |
| 653.0 | 5.900 |
| 675.0 | 5.970 |
| 700.0 | 6.040 |
| 725.0 | 6.100 |
| 750.0 | 6.160 |
| 775.0 | 6.210 |
| 800.0 | 6.244 |
| 825.0 | 6.261 |
| 850.0 | 6.279 |
| 875.0 | 6.296 |
| 900.0 | 6.313 |
| 925.0 | 6.330 |

TABLE D.10

MODEL AF10

| Depth (km) | Shear Velocity (km/sec) |
|---|---|
| 0.0 | 3.200 |
| 3.5 | 3.200 |
| 4.0 | 3.650 |
| 35.0 | 3.650 |
| 38.0 | 4.800 |
| 50.0 | 4.790 |
| 75.0 | 4.775 |
| 100.0 | 4.775 |
| 125.0 | 4.775 |
| 150.0 | 4.775 |
| 175.0 | 4.710 |
| 200.0 | 4.630 |
| 225.0 | 4.640 |
| 250.0 | 4.670 |
| 275.0 | 4.695 |
| 300.0 | 4.720 |
| 325.0 | 4.740 |
| 350.0 | 4.755 |
| 375.0 | 4.765 |
| 404.0 | 4.780 |
| 406.0 | 5.000 |
| 425.0 | 5.050 |
| 450.0 | 5.065 |
| 475.0 | 5.080 |
| 500.0 | 5.140 |
| 525.0 | 5.220 |
| 550.0 | 5.260 |
| 575.0 | 5.300 |
| 600.0 | 5.340 |
| 625.0 | 5.390 |
| 647.0 | 5.480 |
| 653.0 | 5.900 |
| 675.0 | 5.970 |
| 700.0 | 6.040 |
| 725.0 | 6.100 |
| 750.0 | 6.160 |
| 775.0 | 6.210 |
| 800.0 | 6.244 |
| 825.0 | 6.261 |
| 850.0 | 6.279 |
| 875.0 | 6.296 |
| 900.0 | 6.313 |

TABLE D.11

MODEL AF11

| Depth (km) | Shear Velocity (km/sec) |
|---|---|
| 0.0 | 3.700 |
| 9.0 | 3.700 |
| 10.0 | 4.750 |
| 25.0 | 4.750 |
| 50.0 | 4.750 |
| 75.0 | 4.750 |
| 100.0 | 4.750 |
| 125.0 | 4.540 |
| 150.0 | 4.490 |
| 175.0 | 4.470 |
| 200.0 | 4.460 |
| 225.0 | 4.460 |
| 250.0 | 4.480 |
| 275.0 | 4.510 |
| 300.0 | 4.570 |
| 325.0 | 4.630 |
| 350.0 | 4.680 |
| 375.0 | 4.730 |
| 404.0 | 4.780 |
| 406.0 | 5.000 |
| 425.0 | 5.050 |
| 450.0 | 5.065 |
| 475.0 | 5.080 |
| 500.0 | 5.140 |
| 525.0 | 5.220 |
| 550.0 | 5.260 |
| 575.0 | 5.300 |
| 600.0 | 5.340 |
| 625.0 | 5.390 |
| 647.0 | 5.480 |
| 653.0 | 5.900 |
| 675.0 | 5.970 |
| 700.0 | 6.040 |
| 725.0 | 6.100 |
| 750.0 | 6.160 |
| 775.0 | 6.210 |
| 800.0 | 6.244 |
| 825.0 | 6.261 |
| 850.0 | 6.279 |
| 875.0 | 6.296 |
| 900.0 | 6.313 |
| 925.0 | 6.330 |

TABLE D.12

MODEL AF12

| Depth (km) | Shear Velocity (km/sec) |
|---|---|
| 0.0 | 3.700 |
| 9.0 | 3.700 |
| 10.0 | 4.750 |
| 25.0 | 4.750 |
| 50.0 | 4.750 |
| 75.0 | 4.750 |
| 100.0 | 4.750 |
| 125.0 | 4.750 |
| 150.0 | 4.750 |
| 175.0 | 4.550 |
| 200.0 | 4.493 |
| 225.0 | 4.490 |
| 250.0 | 4.530 |
| 275.0 | 4.552 |
| 300.0 | 4.593 |
| 325.0 | 4.647 |
| 350.0 | 4.680 |
| 375.0 | 4.730 |
| 404.0 | 4.780 |
| 406.0 | 5.000 |
| 425.0 | 5.050 |
| 450.0 | 5.065 |
| 475.0 | 5.080 |
| 500.0 | 5.140 |
| 525.0 | 5.220 |
| 550.0 | 5.260 |
| 575.0 | 5.300 |
| 600.0 | 5.340 |
| 625.0 | 5.395 |
| 647.0 | 5.480 |
| 653.0 | 5.900 |
| 675.0 | 5.970 |
| 700.0 | 6.040 |
| 725.0 | 6.100 |
| 750.0 | 6.160 |
| 775.0 | 6.210 |
| 800.0 | 6.244 |
| 825.0 | 6.261 |
| 850.0 | 6.279 |
| 875.0 | 6.296 |
| 900.0 | 6.313 |
| 925.0 | 6.330 |

## REFERENCES


Aki, K., and P.G. Richards, Quantitative Seismology, v.1, W.H. Freeman and Company, New York, 1980.

Anderson, D.L., Thermally induced phase changes, lateral heterogeneity of the mantle, continental roots, and deep slab anomalies, J. Geophys. Res., 92, 13968-13980, 1987.

Anderson, D.L., and J.D. Bass, Mineralogy and composition of the upper mantle, Geophys. Res. Lett., 11, 637-640, 1984.

Bergh, H., Sea-floor spreading in the Southwest Indian Ocean, J. Geophys. Res., 76, 6276-6282, 1971.

Brown, C., and R.W. Girdler, Interpretation of African gravity and its implication for the breakup of the continents, J. Geophys. Res., 85, 6443-6455, 1980.

Burdick, L.J., S.P. Grand, D.V. Helmberger, T. Lay, and J.A. Rial, Remote sensing of attenuation bias using SS, Woodward-Clyde Consultants Technical Report, WCCP-R-83-01, 1983.

Burdick, L.J., and D.V. Helmberger, The upper mantle P velocity structure of the western United States, J. Geophys. Res., 83, 1699-1712, 1978.

Burdick, L.J., and J.A. Orcutt, A comparison of the generalized ray and reflectivity methods of waveform synthesis, Geophys. J. R. Astron. Soc., 58, 261-278, 1979.

Burke, K., Evolution of continental rift systems in the light of plate tectonics, in Tectonics and Geophysics of Continental Rifts, v.2, I.B. Ramberg and E.R. Neumann, Editors, D. Reidel Publishing Co., Dordrecht, Holland, 329-345, 1978.

Burke, K., and J.T. Wilson, Is the African plate stationary?, Nature, 239, 387-389, 1972.

Chapman, D.S., and H.N. Pollack, 'Cold spot' in West Africa: anchoring the African plate, Nature, 250, 477-478, 1974.

Chapman, D.S., and H.N. Pollack, Global heat flow: A new look, Earth Planet. Sci. Lett., 28, 23-32, 1975.

Chapman, D.S., and H.N. Pollack, Regional geotherms and lithospheric thickness, Geology, 5, 265-268, 1977.

Chase, C.G., Extension behind island arcs and motions relative to hot spots, J. Geophys. Res., 83, 5385-5387, 1978.

Elsasser, W.M., Sea-floor spreading as thermal convection, J. Geophys. Res., 76, 1101-1112, 1971.

Forsyth, D., and S. Uyeda, On the relative importance of the driving forces of plate motion, Geophys. J. R. Astro. Soc., 43, 163-200, 1975.

Gass, I.G., Tectonics and magmatic evolution of the Afro-Arabian dome, in African Magmatism and Tectonics, T.N. Clifford and I.G. Gass, Editors, Oliver and Boyd, Edinburgh, 285-300, 1970.

Girdler, R.W., The great negative Bouguer anomaly over Africa, EOS Trans. Am. Geophys. Union, 56, 516-519, 1975.

Girdler, R.W., Comparison of the East African Rift system and the Permian Oslo Rift, in Tectonics and Geophysics of Continental Rifts, v.2, I.B. Ramberg and E.R. Neumann, Editors, D. Reidel Publishing Co., Dordrecht, Holland, 329-345, 1978.

Girdler, R.W., Processes of planetary rifting as seen in the rifting and break up of Africa, Tectonophysics, 94, 241-252, 1983.

Given, J.W., Inversion of body-wave seismograms for upper mantle structure, Ph.D Thesis, 154 pp., Calif. Inst. of Technol., Pasadena, 1984.

Gordon, R.G., A. Cox, and C.E. Harter, Estimation of the absolute motion of an individual plate from its ridge and trench boundaries, Nature, 274, 752-755, 1978.

Gordon, R.G., and D.M. Jurdy, Cenozoic global plate motions, J. Geophys. Res., 91, 12389-12406, 1986.

Gordon, R.G., M.O. McWilliams, and A. Cox, Pre-Tertiary velocities of the continents: a lower bound from paleomagnetic data, J. Geophys. Res., 84, 5480-5486, 1979.

Grand, S.P., Shear velocity structure of the mantle beneath the North American plate, Ph.D Thesis, 228 pp., Calif. Inst. of Technol., Pasadena, 1986.

Grand, S.P., Tomographic inversion for shear velocity beneath the North American plate, J. Geophys. Res., 92, 14065-14090, 1987.

Grand, S.P., D.V. Helmberger, and L.J. Burdick, 1985, Attenuation bias measurements of the Semipalatinsk and North African test sites, Woodward-Clyde Consultants Technical Report, WCCP-R-85-01, 1985.

Jordan, T.H., The continental tectosphere, Rev. Geophys. Space Phys., 13, 1-12, 1975.

Jordan T.H., Composition and development of the continental tectosphere, Nature, 274, 544-548, 1978.

Jurdy, D.M., and R.G. Gordan, Global plate motions relative to the hot spots 64 to 56 Ma, J. Geophys. Res., 89, 9927-9936, 1984.

Lerner-Lam, A.L., and T.H. Jordan, How thick are the continents?, J. Geophys. Res., 92, 14007-14026, 1987.

Logatchev, N.A., Y.A. Zorin, and V.A. Rogozhina, Baikal Rift: active or passive?-comparison of the Baikal and Kenya rift zones, Tectonophysics, 94, 223-240, 1983.

McKenzie, D., Active tectonics of the Mediterranean region, Geophys. J. R. Astron. Soc., 30, 109-185, 1972.

Mimouni, A., and M. Rabinowicz, The old continental shields stability related to mantle convection, Geophys. Res. Lett., 15, 68-71, 1988.

Minster, J.B., T.H. Jordan, P. Molnar, and E. Haines, Numerical modelling of instantaneous plate tectonics, Geophys. J. R. Astron. Soc., 36, 541-576, 1974.

Nolet, G., and S. Mueller, A model for the deep structure of the East African Rift system from simultaneous inversion of teleseismic data, Tectonophysics, 84, 151-178, 1982.

Okal, E.A., and D.L. Anderson, A study of lateral inhomogeneities in the upper mantle by multiple ScS travel-time residuals, Geophys. Res. Lett., 2, 313-316, 1975.

Oxburgh, E.R., and D.L. Turcotte, Membrane tectonics and the East African Rift, Earth Planet. Sci. Lett., 22, 133-140, 1974.

Pollack, H.N., and D.S. Chapman, On the regional variation of heat flow, geotherms, and lithospheric thickness, Tectonophysics, 38, 279-296, 1977.

Rial, J.A., S.P. Grand, and D.V. Helmberger, A note on the lateral variation in upper-mantle shear structure across the Alpine front, Geophys. J. R. Astron. Soc., 77, 639-655, 1984.

Richardson, R.M., S.C. Solomon, and N.H. Sleep, Tectonic stress in the plates, Rev. Geophys. Space Phys., 17, 981-1019, 1979.

Sengor, A.M.C., and K. Burke, Relative timing of rifting and volcanism on earth and its tectonic implications, Geophys. Res. Lett., 5, 419-421, 1978.

Sheriff, R.E., and L.P. Geldart, Exploration Seismology, v.1, Cambridge University Press, Cambridge, 1982.

Sipkin, S.A., and T.H. Jordan, Lateral heterogeneity of the upper mantle determined from travel times of ScS, J. Geophys. Res., 80, 1474-1484, 1975.

Sipkin, S.A., and T.H. Jordan, Lateral heterogeneity of the upper mantle determined from the travel times of multiple ScS, J. Geophys. Res., 81, 6307-6320, 1976.

Solomon, S.C., and N.H. Sleep, Some simple physical models for absolute plate motions, J. Geophys. Res., 79, 2557-2567, 1974.

Solomon, S.C., N.H. Sleep, and D.M. Jurdy, Mechanical models for absolute plate motions in the early Tertiary, J. Geophsy. Res., 82, 203-212, 1977.

Thorpe, R.S., and K. Smith, Distribution of Cenozoic volcanism in Africa, Earth Planet. Sci. Lett., 22, 91-95, 1974.

Toksöz, M.N., and D.L. Anderson, Phase velocities of long-period surface waves and structure of the upper mantle, J. Geophys. Res., 71, 1649-1658, 1966.

Turcotte, D.L., and G. Schubert, Geodynamics, John Wiley and Sons, New York, 1982.

Vitorello, I., and H.N. Pollack, On the variation of continental heat flow with age and the thermal evolution of continents, J. Geophys. Res., 85, 983-995, 1980.

Wald, D.J., and T.C. Wallace, A seismically active section of the Southwest Indian Ridge, Geophys. Res. Lett., 13, 1003-1006, 1986.

Woodhouse, J.H., and A.M. Dziewonski, Mapping the upper mantle: three-dimensional modeling of earth structure by inversion of seismic waveforms, J. Geophys. Res., 89, 5953-5986, 1984.